ACS OMEGA

http://pubs.acs.org/journal/acsodf

Article

Pore Structure and Movable Fluid Characteristics of Typical Sedimentary Lithofacies in a Tight Conglomerate Reservoir, Mahu Depression, Northwest China

Jianbang Wu, Shenglai Yang,* Bowen Gan, Yushun Cao, Wei Zhou, Gen Kou, Ziqiang Wang, Qiang Li, Wengang Dong, and Binbin Zhao

Cite This: *ACS Omega* 2021, 6, 23243−23261

Read Online

ACCESS | Metrics & More | Article Recommendations

ABSTRACT: The pore structure and movable fluid characteristics of tight conglomerate reservoirs are complex, which are greatly different from conventional reservoirs. The depositional mechanism is the fundamental factor controlling the physical properties of conglomerate reservoirs. However, there is a lack of systematic research on the pore structure and movable fluid characteristics of conglomerate reservoirs with typical sedimentary facies. This paper investigates the pore structure and movable fluid characteristics of conglomerate of different sedimentary facies based on various experiments. Casting thin sections, X-ray diffraction, scanning electron microscopy, high-pressure mercury injection, and nuclear magnetic resonance experiments were conducted on 32 conglomerates samples from the Mahu Sag, Junggar Basin, China. The quality classification method of tight conglomerate reservoirs is established. The results show that the conglomerate can be divided into three sedimentary facies; traction flow conglomerate (TFC) and pebbled sandstone (PSS) mainly develop intergranular pores and dissolved pores; and the pore diameter curves are mainly a double peak, single peak, and flat peak. Gravity flow conglomerate (GFC) mainly develops dissolved pores and interstitial micropores, and the pore diameter curve is mainly a single peak. PSS includes pebbled gritty sandstone (P(G)SS) and pebbled fine sandstone (P(F)SS). TFC and P(G)SS are favorable class I reservoirs, while GFC and P(F)SS are nonfavorable class II reservoirs. A new parameter, the ratio of the major axis to the minor axis of the pore outer ellipse (axial ratio), is proposed to quantitatively describe the compaction effect. The average axial ratios of the three lithofacies are 3.04, 3.98, and 8.78, respectively, indicating that the compaction is intensified and the pore structure becomes worse. By analyzing the correlation between pore structure parameters and permeability, it is found that the main controlling factors of permeability of GFC and TFC are sorting and connectivity, respectively, and the main flow radius is the most suitable parameter to describe permeability. A linear spectral decomposition method was used to establish a new quantitative calculation method of movable fluid saturation for different types of pores, and the results show that the movable fluid saturation of intergranular pores is the highest (average: 65.43%), and the movable fluid saturation of TFC and P(G)SS with more intergranular pores is the highest. Movable fluid saturation is inversely proportional to the content of I/S and the compaction rate and positively proportional to the content of quartz and feldspar and the cementation rate. The fluid mobility of water-wet samples is weaker. The research results provide theoretical support for the identification of favorable reservoirs and the cognition of a development mechanism.

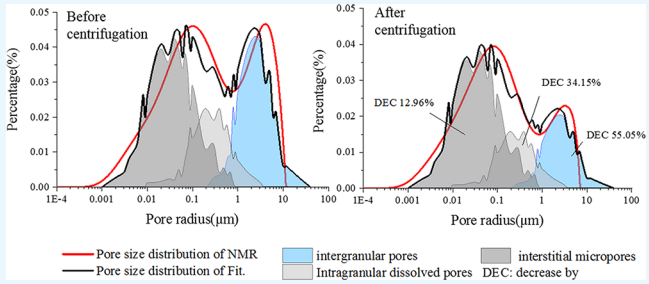

1. INTRODUCTION

Conglomerate reservoirs are widely developed around the world. With the increasing degree of oil and gas exploration, conglomerate reservoirs have attracted widespread attention.[1,2] In recent years, a super-large conglomerate reservoir of 1 billion tons has been discovered in the Mahu Sag, which has become the main area of Xinjiang oilfield to increase production.[3] Although the Mahu block is rich in reserves, due to its unique sedimentary characteristics and accumulation characteristics, on the basis of tight reservoirs, it also has the characteristics of near provenance, complex lithology, and strong heterogeneity. Development is relatively more difficult. The lithofacies division, physical properties, pore structure, fluid mobility, and favorable reservoir division of conglomerate reservoirs have been unresolved. At present, the block has encountered difficulties in understanding the mechanism of fracturing reform and rolling

Received: June 6, 2021
Accepted: August 24, 2021
Published: September 2, 2021

development. It is urgent to conduct new and more in-depth evaluation and research on the above problems from the perspective of sedimentary genesis.[4,5]

Lithofacies is a rock or rock combination formed in a certain sedimentary environment that can reflect the hydrodynamic conditions during deposition, and hydrodynamic conditions and diagenetic transformation are important factors affecting physical properties. Miall pointed out that the unified analysis of the sedimentary structure and lithology of rocks is more practical and is the trend of reservoir research.[6,7] The lithofacies classification of conglomerate has been controversial, and the lithofacies classification of conglomerate has always been divided, but the research process does reflect the development trend from simple lithology to sedimentary lithofacies; Cant and Ethier divided the conglomerate in the Elmworth gas field in Canada into three lithologies and believed that the physical properties of the conglomerate with a single grain structure are better than the two-stage grain structure and the sandy conglomerate.[8] Hart and Pint and Ernando and Fathoni divided conglomerate into conglomerate and conglomerate sandstone[9,10] and explained that the physical properties of the reservoir depend on the content of the matrix and pore structure; Zhang et al. divided the conglomerate into six categories, such as single peak, double peak, and multi-peak, according to the pore size mode, and believed that the sedimentary mechanism was the fundamental factor determining the difference in physical properties;[11] Wang and Mao proposed that diagenesis is an important factor affecting the homogeneity of conglomerate reservoirs;[12] Zhang et al. pointed out that sedimentary characteristics are closely related to the support structure of conglomerates and have important petroleum geological significance.[13] The current research is mostly based on the classification of particle types and pore throat distribution and does not reflect the cause mechanism, which is not conducive to finding favorable layers and explaining the development phenomenon. Some scholars recognize that the content of matrix and the characteristics of pore throats have a greater impact on physical properties, but they did not consider the sedimentary genesis nor did they realize that the complex and diverse conglomerates can be classified from the perspective of genesis from the perspective of sedimentary mechanism. There is a lack of in-depth analysis of reservoir physical properties, pore throat structure, movable fluids, etc. of different sedimentary genesis and lithofacies. On the basis of previous studies, starting from the sedimentary mechanism and assisted by the characteristics of grain structure, this study systematically evaluated and studied the physical properties of different sedimentary facies in the conglomerate reservoir.

The research methods for the pore throat structure of tight reservoirs are relatively mature, and the focus is on the choice of different experimental methods.[15,16] Nuclear magnetic resonance (NMR) is a fast and nondestructive technique that measures the T_2 relaxation time of fluid clusters of different scales in porous media to obtain petrophysical properties and the fluid occurrence status. It is widely used in porosity calculations and permeability and movable fluid content evaluation.[14,17] The Mahu conglomerate reservoir has less ferromagnetic materials and larger particles, which is suitable for preparing large-size samples for testing, and NMR is an ideal method for testing its pore throat structure. The key to the test is to determine the conversion relationship between T_2 and the pore radius. The similarity method is currently the best method to determine the conversion coefficient, that is, to determine the conversion coefficient by comparing and fitting the PSD obtained from other experiments.[18,19] Since NMR measures the signal of the fluid that is pressed into the pores under high pressure, the high-pressure mercury injection (HPMI) method can best reflect the pore distribution of the pressed fluid, and the HPMI method can obtain abundant pore structure information;[20−23] therefore, this paper uses the HPMI-NMR method to jointly test the pore throat structure of conglomerate samples; evaluates the influence of the pore homogeneity, sorting, connectivity, and other parameters on the physical properties of the reservoir of different lithofacies samples; and uses the NMR-centrifugal method to test the movable fluid condition of the core.[17,24]

The pore type and pore morphology can best reflect the controlling effect of the sedimentary genesis of different lithofacies. In the past, the analysis of compaction and other diagenesis was mostly based on the analysis of cuttings, few studies can quantitatively characterize the impact of compaction on pore morphology, the traditional method of using the equivalent circle radius to characterize the pore size neglected the difference in pore morphology, and the important parameters of the influence of reaction sedimentary diagenesis are missed.[25,26] The type of pore throat has a significant effect on fluid fluidity, but it is difficult to quantitatively describe the movable fluid in different types of pores. The main types of pores developed in different sedimentary facies are diverse, and the pore throat configuration relationship is different. Due to the attachment and blockage of clay minerals, various types of pores will form a seepage network with various structures, which has a direct impact on the mobility of the occurrence fluid.[27−29] Previous studies have often neglected the influence of pore types on movable fluids, some studies simply set a T_2 spectrum value in the NMR pore distribution to represent the boundary of different types of pores,[30,31] but most of the pore sizes of different types have crossed. Cast thin sections and scanning electron microscopy (SEM) methods can more accurately measure the distribution characteristics of different types of pores,[32,33] but the experimental results have difficulty in establishing a relationship with the pore parameters obtained by NMR. In the field of remote sensing, there is a method of spectral decomposition,[34,35] which can calculate the proportion of a single spectrum under the condition of known mixed spectra. If the pore size distribution (PSD) obtained by NMR is regarded as a combination of different types of pores and the PSD of NMR and the distribution of various types of pores have been known, then using the idea of spectral decomposition, the proportion of each type of pore can be obtained so as to obtain the degree of flow utilization in each type of pore before and after centrifugation. Therefore, on the basis of casting thin section and SEM experiments, this research first uses microscopic pore photos to perform morphological analysis to identify the size distribution, face ratio, pore circumference, circumscribed ellipse axis length, shape factor, and other parameters of different types of pores; obtain rich data that can reflect the effect of diagenesis and then use the distribution of various types of pores to scale the pore distribution obtained by NMR-centrifugation; and more accurately quantify the fluid movement in different types of pores. In addition, geological control factors have an important influence on fluid mobility.[30] Mineral types, compaction, cementation, wettability, and other geological control parameters are closely related to the saturation of movable fluids, but there is a lack of relevant research. This study will further analyze the influence of geological control on the

https://doi.org/10.1021/acsomega.1c02952
ACS Omega 2021, 6, 23243−23261

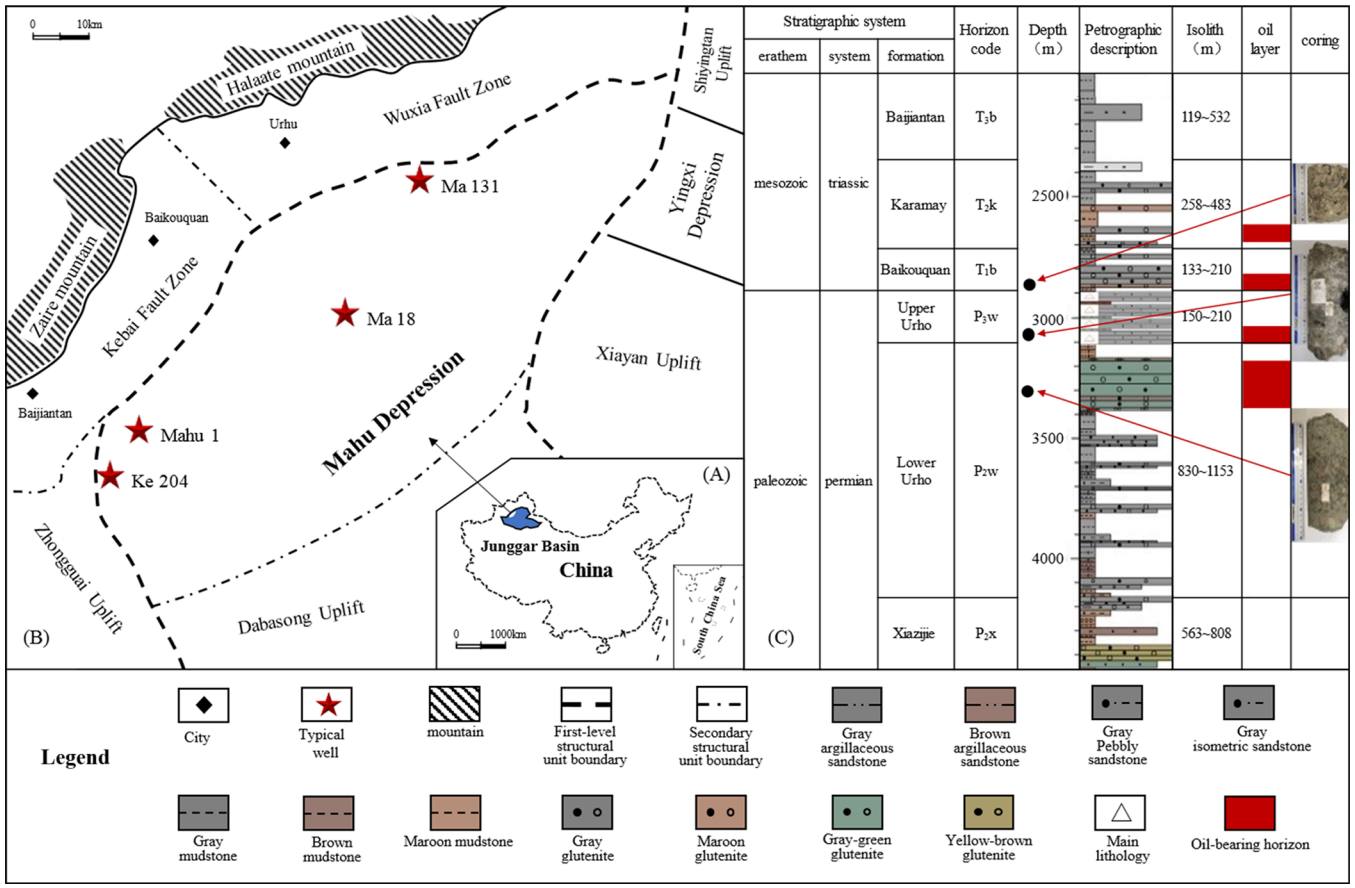

Figure 1. Geological survey of the study area. (A) Location of the Junggar Basin. (B) Tectonic units contained in the northwestern margin of the Junggar Basin. (C) Stratigraphic distribution of the study area and core-taking of the study samples.

saturation of movable fluids based on the differences in sedimentation and diagenesis of different lithofacies samples.

In this study, first, core observations, porosity, and permeability tests were conducted on 94 cores of Wuerhe–Baikouquan Formation in Mahu Depression, and different sedimentary facies such as gravity flow origin and traction flow origin were classified according to sedimentary facies belts, then NMR, HPMI, cast thin section, SEM, X-ray diffraction (XRD), and other methods were tested on 32 typical rock samples, and the petrological characteristics, pore types, pore size distribution, and structural characteristics of different sedimentary facies samples were obtained, and then we analyzed the influence of sedimentary diagenesis mechanism and pore structure on the quality of reservoirs in each lithofacies, quantitatively evaluated the influence of pore types and clay minerals on movable fluids, and classified favorable reservoirs based on this.

2. GEOLOGIC SETTING

The northwestern margin of the Junggar Basin is an important oil and gas production area, which structurally includes the Kebai fault zone, the Wuxia fault zone, and the Mahu Sag, including parts of the Dabasong, Xiayan, and Zhongguai swells (Figure 1A,B). The southern slope of the Mahu Sag in the study area is a large monoclinic structure as a whole, with the strata inclined to the southeast.[36] There are nearly east–west trending faults in this area. This group of faults was formed in the Indosinian period, and some of them were reactive in the Himalayan period, mainly formed by the compression and torsional shear stress during the sag development period. The faults are mainly strike-slip with a parallel distribution and steep section.[37,38]

The Manan slope area is relatively well-developed, from bottom to top, and they are the Permian Jiamuhe Formation, Fengcheng Formation, Xiazijie Formation, Upper Wuerhe Formation, Lower Wuerhe Formation, Triassic Baikouquan Formation, Karamay Formation, and Baijiantan Formation (Figure 1C). The research horizon in this paper is from the Upper Wuerhe Formation of the Permian to the Baikouquan Formation of the Triassic. Due to the continuous decline of the basement of the descending plate of the large fault on the northwestern margin of the Junggar Basin, the steep slope side is adjacent to the provenance, and the detrital material is transported by intermittent flooding and seasonal rivers in a short distance. A large set of fan delta plain subfacies conglomerate and conglomerates bodies are deposited on the edge of the basin, and fan delta front subfacies conglomerates, conglomerate sandstone, and sandstone are deposited toward the center of the lake basin. The total thickness of the reservoir exceeds 1500 m.[39,40] Therefore, the research layer lithology is dominated by gray, gray-green, and brown conglomerates and pebbly sandstone (Figure 1C), with typical conglomerates sedimentary microfacies such as debris flow/clastic flow, braided channel, underwater distributary channel, fan channel, etc. Conglomerates modalities are significantly different, and sedimentation and diagenesis have an important impact on reservoir development.[41,42]

https://doi.org/10.1021/acsomega.1c02952
ACS Omega 2021, 6, 23243−23261

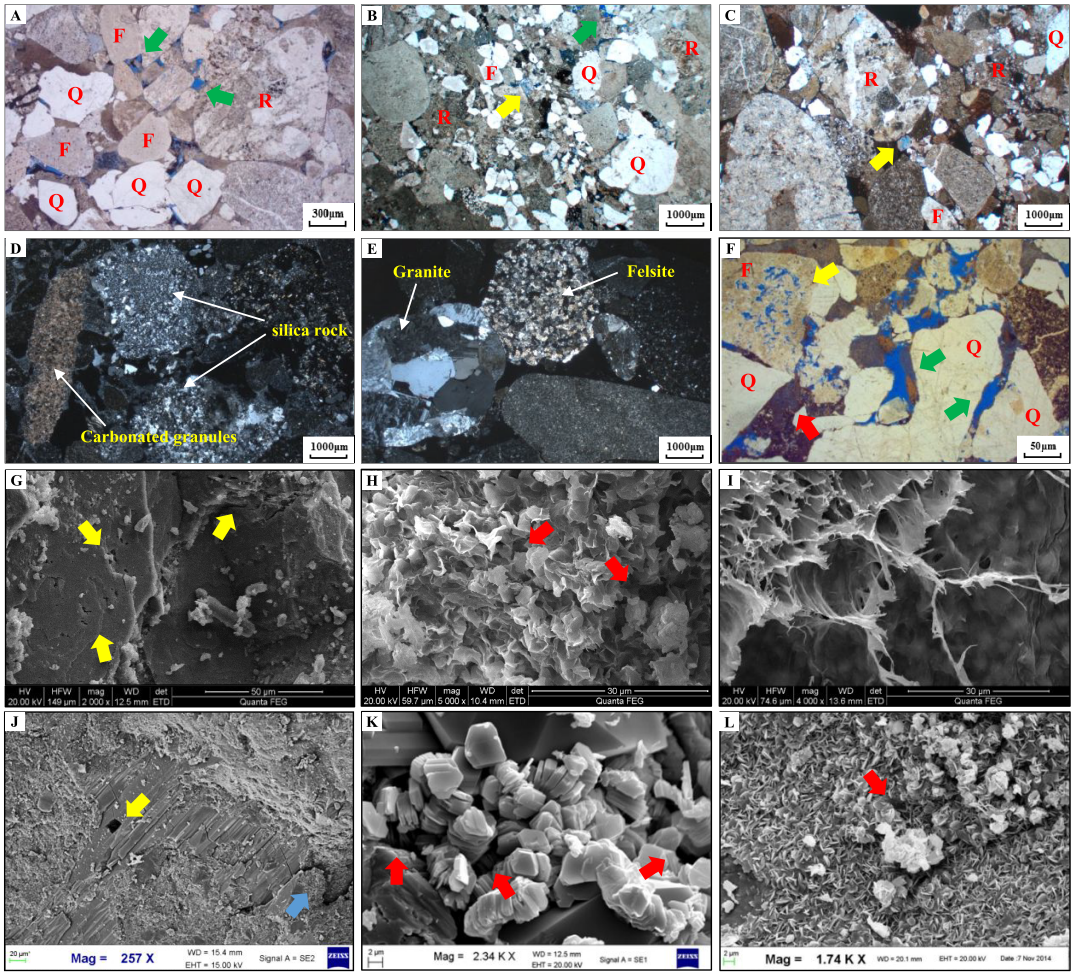

Figure 2. Typical lithofacies, pore types, and petrological characteristics of the Mahu conglomerate reservoir. (A) Traction flow conglomerate. (B) Pebbled sandstone. (C) Gravity flow conglomerate. (D) Carbonate minerals and siliceous detritus. (E) Granite and felsic clasts. (F) Typical pore types in the cast thin section under a microscope. (G) Dissolved pores developed in feldspar. (H) Irregular immongous intergranular layer and honeycomb intergranular pore on the grain surface. (I) Granular silky illite. (J) Zeolite minerals dissolved pores. (K) Intergranular filling of worm-like kaolinite and intercrystalline pores. (L) Leaf chlorite and intercrystalline pores on the surface of grains (letter Q: quartz; F: feldspar; R: Gravel fragments). Green arrows in the image indicate intergranular pores. Yellow arrows: dissolved pores in grains; red arrows: interstitial.

3. EXPERIMENTAL SECTION

3.1. Sample Preparation. In this study, a total of 94 plunger-shaped core samples were obtained from four wells with a depth ranging from 3205 to 3623 m. These samples were prepared parallel to the bedding. First, the rock sample was cleaned, dried at 110 °C, and then tested for helium porosity and gas permeability. Thirty-one typical samples were selected, and XRD, SEM, HPMI, NMR, and centrifugal experiments were carried out.

3.2. Experimental Methods. SEM and XRD experiments were carried out under a Quanta 200, ZEISS MERLIN high-resolution FE-SEM and D8 X-ray diffractometer according to GB/T 16594-2008 and SY/T 5163-2010 standards. The laboratory temperature was 20 °C, and the humidity was <80%. Observation and analysis of minerals, particle size, and pores are carried out based on the images under a microscope. Pores (12,653) were analyzed and measured with ImageJ, MATLAB, and Photoshop software. The pore types were classified according to the genetic characteristics, and the pore shape parameters were extracted and calculated.

The HPMI experiment was carried out on an American corelab CMS300 and AutoPore IV 9505 mercury porosimeter according to the GB/T29171-2012 standard. The samples were dried at 105 °C to constant weight before testing, and the maximum experimental pressure was 200 MPa. Based on the capillary model, the mercury intrusion curve and Washburn equation were used to obtain the pore size distribution and related structural parameters.

The NMR experiment was carried out on an SPEC-SC1 nuclear magnetic resonance core analyzer according to the SY/T 6490-2014 standard. The parameters were set as follows: the number of scans: 64, the waiting time: 5000 ms, the number of acquisition points: 10240, the pulse interval: 80 μs.

In this paper, the HPMI pore diameter distribution of the same core is used to scale the NMR data by the method of Li et al:[43] (1) The power exponential relationship between the transverse relaxation time T_2 and pore diameter r in the saturated oil channel of a spherical cylinder in a uniform magnetic field was obtained: $r = C \times T_2^{1/n}$, where C and n are the fitting coefficients. (2) The cumulative distribution frequencies of the mercury injection pore radius R and T_2 relaxation time were plotted respectively. (3) R and T_2 with the same cumulative frequency were obtained by interpolation, and the power exponential function was fitted by the least square method. The

https://doi.org/10.1021/acsomega.1c02952
ACS Omega 2021, 6, 23243−23261

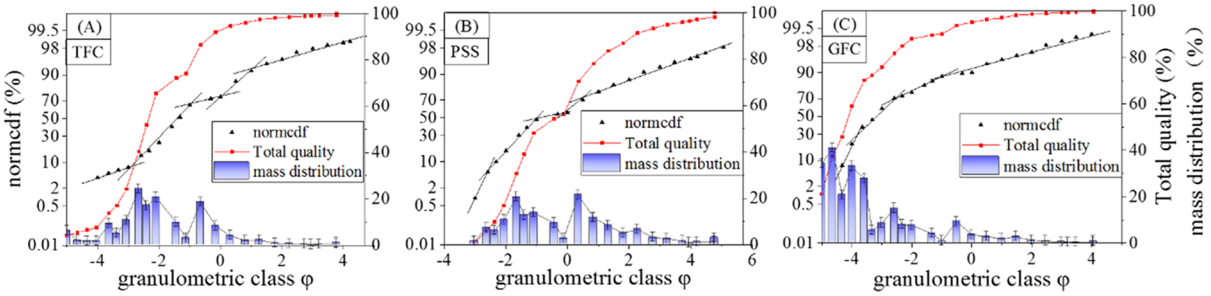

Figure 3. The particle size distribution map of the conglomerate sample includes the grain size distribution and cumulative probability curve. Panels (A–C) are the particle size distribution maps of traction flow conglomerate, pebbled sandstone, and gravity flow conglomerate, respectively. The accumulative probability curve of particle size of traction flow deposition is two-stage or multi-stage, and the particle size is a two-peak or multi-peak distribution of small pebbles. The accumulative probability curve of particle size of gravity flow deposition shows a steeper slope and a gentle upward arc, and the particle size is a single-peak distribution of medium pebbles.

conversion coefficients C and n are thus obtained. The centrifugal experiment was carried out on a Cence-H1850 centrifuge, with a maximum speed of 9000 rpm and a pressure difference of about 3.6Mpa. The original dry state, saturated *n*-dodecane, and centrifugal state of the same batch of rock samples were tested by NMR.

3.3. Lithofacies Classification. According to the logging data and core data of the study block, a large set of fan delta facies sandstone reservoir was developed in Baikouquan and Wuerhe Formations in the south slope area of Mahu Basin, which can be divided into traction flow and gravity flow according to the sedimentary origin, among which the traction flow origin is composed of both gravel sandstone and gravel conglomerate; for the conglomerate reservoirs with complex modes, the classification of particle size and support structure can be avoided in this way, and the fundamental factors that affect the physical characteristics of rocks can be captured through sedimentary genesis. The lithofacies are described as follows:[11,44]

(1) The traction flow conglomerates facies (TFC) is developed at the bottom of the fan channel microfacies of the fan delta plain subfacies and the underwater distributary channel microfacies of the fan delta front subfacies. It is formed by the normal traction flow during the intercatastrophic period, it has obvious cross bedding and parallel bedding, and the cumulative probability curve of particle size of traction flow deposition is a typical two-stage or multi-stage.

(2) Gravity flow conglomerates facies (GFC) developed in the debris flow microfacies of the fan delta plain subfacies, and the detrital flow microfacies of the fan delta front subfacies, formed by catastrophic events, developed massive bedding and mixed structure. The cumulative probability curve of particle size shows a steeper slope and a gentle upward arc.

(3) Pebbly sandstone facies (PSS) are mostly formed under the action of traction currents, mainly developed on the top of fan channel microfacies and underwater distributary channel microfacies and may develop oblique bedding, parallel bedding, cross bedding, etc. Typical pebbly sandstone includes pebbly gritty sandstone (P(G)SS) and pebbly fine sandstone (P(F)SS).

4. RESULTS

4.1. Grain Size Distribution and Petrological Characteristics. The classification of conglomerate in sedimentology research is based on the classification of sand and mudstone. Krumbein uses a simple integer Φ value to represent the particle size of the debris particles[45] ($\Phi = -\log_2 D$, D is the particle diameter/mm). As shown in Figure 3, the particle size distribution of traction flow deposition conglomerate shows a two-peak or multi-peak distribution, indicating the existence of a two-stage or multi-stage particle support. The size of TFC is concentrated in φ = [−4 to 0] means that the particle size is in a range of 1−16 mm, with an average of 1.86 mm, mainly fine gravel. The size of PSS is concentrated in φ = [−2 to 2], that is, the particle size is in a range of 0.25−4, with an average of 1.05 mm, mainly gravel and sand. The particle size of GFC is mostly unimodal, concentrated in φ = [−5 to −2], that is, the particle size is in a range of 4−30 mm, with an average of 5.85 mm, mainly in gravel.

According to the analysis and statistics of casting thin sections and XRD, the gravel composition of the sample is mainly magmatic rock and metamorphic rock, mainly including tuff (42.67%), granite (18.4%), quartz (3.12%), etc. (Figure 2A–E). GFC is mostly formed in catastrophic sedimentary environments. Gravels are mostly floating, with very poor sorting, poor roundness to medium, and low maturity. The interstitial materials are mainly muddy impurities. TFC is mainly subjected to normal water flow elutriation, and it is good in maturity and roundness, and the content of argillaceous impurities is low. The sedimentary environment characteristics of PSS are similar to those of TFC, and gravel and sandy particles are in contact with each other (Figure 2A–C). Sandy conglomerate cement is dominated by calcite, and the types of cementations are press-embedded and pore-press-embedded. The particles are mainly in point-line contact and line contact. The argillaceous heterogroups underwent varying degrees of hydromica and kaolinization. The argillaceous content of the samples averaged 4.5%, and the clay minerals can be observed in illite/smectite mixed layers (I/S), illite, kaolinite, chlorite, etc. (Figure 2H,I,K,L). Among them, there are more I/S mixed layers with an average of 56.0% followed by kaolinite (K) (16.7%) and illite (I) (16.5%), with a small amount of chlorite (C).

4.2. Reservoir Physical Properties and Oil-Bearing Properties. Mahu conglomerate reservoir samples have low porosity and permeability and strong heterogeneity. As shown in Figure 4A, the overall porosity distribution ranges from 2.31 to 13.17%, with an average of 7.096% and a mid-value of 6.0%; the overall permeability distribution ranges from 0.005 to 6.37 mD, with an average of 0.749 mD and a mid-value of 0.3 mD; the reservoir porosity and permeability are basically positively correlated. The physical properties of conglomerates from different sedimentary genes are quite different. TFC has better physical properties, with an average porosity of 9.85%, ranging from 6.15 to 14.54%, and an average permeability of 1.32 mD,

https://doi.org/10.1021/acsomega.1c02952
ACS Omega 2021, 6, 23243−23261

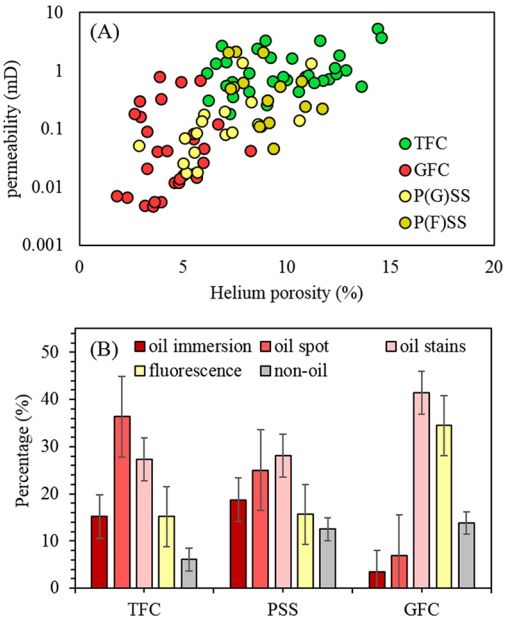

Figure 4. Physical properties and oil-bearing characteristics of the three lithofacies. Panel (A) is the cross plot of porosity and permeability; panel (B) is the proportion chart of various oil-bearing samples. The average porosities of TFC, PSS, and GFC are 9.85, 7.77, and 4.14%, and the average permeabilities are 1.32, 0.47, and 0.13 mD, respectively. The overall reservoir is tight, the physical property becomes worse in turn, and the oil content decreases in turn.

ranging from 0.18 to 5.38 mD. The physical properties of GFC are poor. The average porosity is 4.14%, and the distribution is between 1.79 and 8.26%. The average permeability is 0.13 mD, and the distribution is between 0.0047 and 0.79 mD. The PSS reservoir has good physical properties, slightly worse than TFC. PSS has a wide range of porosity and permeability, and the overall physical properties of P(G)SS are better than P(F)SS. The porosity of GFC core is obviously low, but the permeability difference can reach dozens of times. The physical properties of tight conglomerates are complex, and further research is needed from the aspects of the diagenesis process and pore structure.

The differences in physical properties between conglomerates of different sedimentary origins determine the differences in oil content (Figure 4B). GFC has very poor oil content, and the oil content is concentrated in the "oil stain-fluorescence" level; the oil content of TFC and PSS is obviously relatively good, and most of the oil content is concentrated in the "oil immersion-oil spot" grade.

4.3. Pore Types and Pore Structures under the Microscope. From the physical meaning of the effect on seepage, three common types of pores can be observed in the research samples (Figure 2A−C,F−H,J−L): intergranular pores (interG-Ps) formed by mutual support of hard particles, intragranular pores (intraG-Ds) caused by the internal dissolution of unstable mineral particles (quartz, feldspar, etc.), and interstitial micropores (interS-Ms) caused by the original or dissolution in the matrix and cement. The pore types of TFC and PSS are mainly native interG-Ps followed by intraG-Ds; GFC pore types are mainly intraG-Ds, and there are a large number of interS-Ms.

According to the experimental results under the microscope, the area and quantity of the different types of pores in the three lithofacies are quantitatively characterized. The area contribution represented by dS/dD can weaken the influence of the number of data points.[46] As shown in the Figure 5, it can be concluded as follows: (1) Overall view, as the pore size increases, the number of pores decreases, while the area of the pores increases. A smaller number of large pores occupy most of the storage space. (2) The pore size distribution of different types of pores is different, and the interG-Ps are mostly above 1 μm. There are concentrated distributions in the interval of about 5 μm, intraG-Ds are mostly distributed in 0.3−3 μm, and interS-Ms are mostly small pores below 1 μm. (3) In different lithofacies, these types of pores have different distributions. The environment where TFC is located has strong hydrodynamics, which is conducive to the preservation of original interstices and concentrates the distribution of interG-Ps; PSS is located in the near provenance zone or the top of sedimentary microfacies, and the content of interG-Ps is less due to the filling of matrix; GFC is generated in catastrophic environments, the original interstices are completely filled, and micropores dominated by intraG-Ds and interS-Ms are mainly distributed. The following uses HPMI and NMR to further analyze the pore distribution and structural characteristics.

4.4. HPMI and NMR Analyses. High-pressure mercury intrusion technology is extensively used to determine the total pore volume and pore size distribution of reservoir rocks.[47] As shown in Figure 6A−C, the capillary force curves of mercury injection samples in the study area mostly conform to the types of II, IV, and V of six typical capillary force curves,[48] and the curve shape of different lithofacies is obviously different. The capillary pressure curves of TFC and PSS are mostly between II and V, which are characterized by an uneven middle section, poor pore sorting, and heterogeneous distribution of rock pore and throat but low mercury injection threshold pressure. Mostly lower than 2 MPa, the pore size is relatively large, but some samples have obvious trapping hysteresis effects, indicating that there is a narrow roar, which forms a shielding effect on retained mercury. The curve of GFC is similar to type IV and type V. There are two typical forms, one is relatively flat in the middle, but the threshold pressure of mercury injection is very high, some even exceed 10 MPa, and there are relatively homogeneous tiny pores; in the other one, the threshold pressure is lower, but the middle section is sharp and the maximum mercury saturation is low (48.9%). This type of reservoir has worse pore sorting and connectivity, tiny pores, and difficult fluid flow.

The T_2 spectrum curve of NMR scaled by HPMI data can reflect the core's comprehensive pore distribution. The pore distribution of conglomerates under NMR shows a diverse morphology. As shown in the Figure 6D−K, the pores of TFC have a wide distribution range, between 0.001 and 10 μm. The curve shape shows a typical double peak exhibiting a slightly smaller or greater slanting degrees, and the peak position of the right peak formed by large pores is mostly above 1 μm; PSS has a complex support structure and particle mode, so the pore distribution forms are multiple. P(G)SS is mostly bimodal showing slightly smaller slanting degrees, unimodal showing greater slanting degrees or flat peak, and P(F)SS is bimodal, multimodal, and unimodal showing previously smaller slanting degrees. Its right peak position is below 2 μm in most cases; GFC pores are narrow, mostly unimodal of small pores or bimodal showing a distinct smaller slanting degrees, and the left peak position is mostly below 0.01 μm, the largest pore of some samples is less than 0.1 μm, and some have a larger right peak position, which may be related to the microcracks generated at the weak point of the gravel edge cementation.[49]

https://doi.org/10.1021/acsomega.1c02952
ACS Omega 2021, 6, 23243−23261

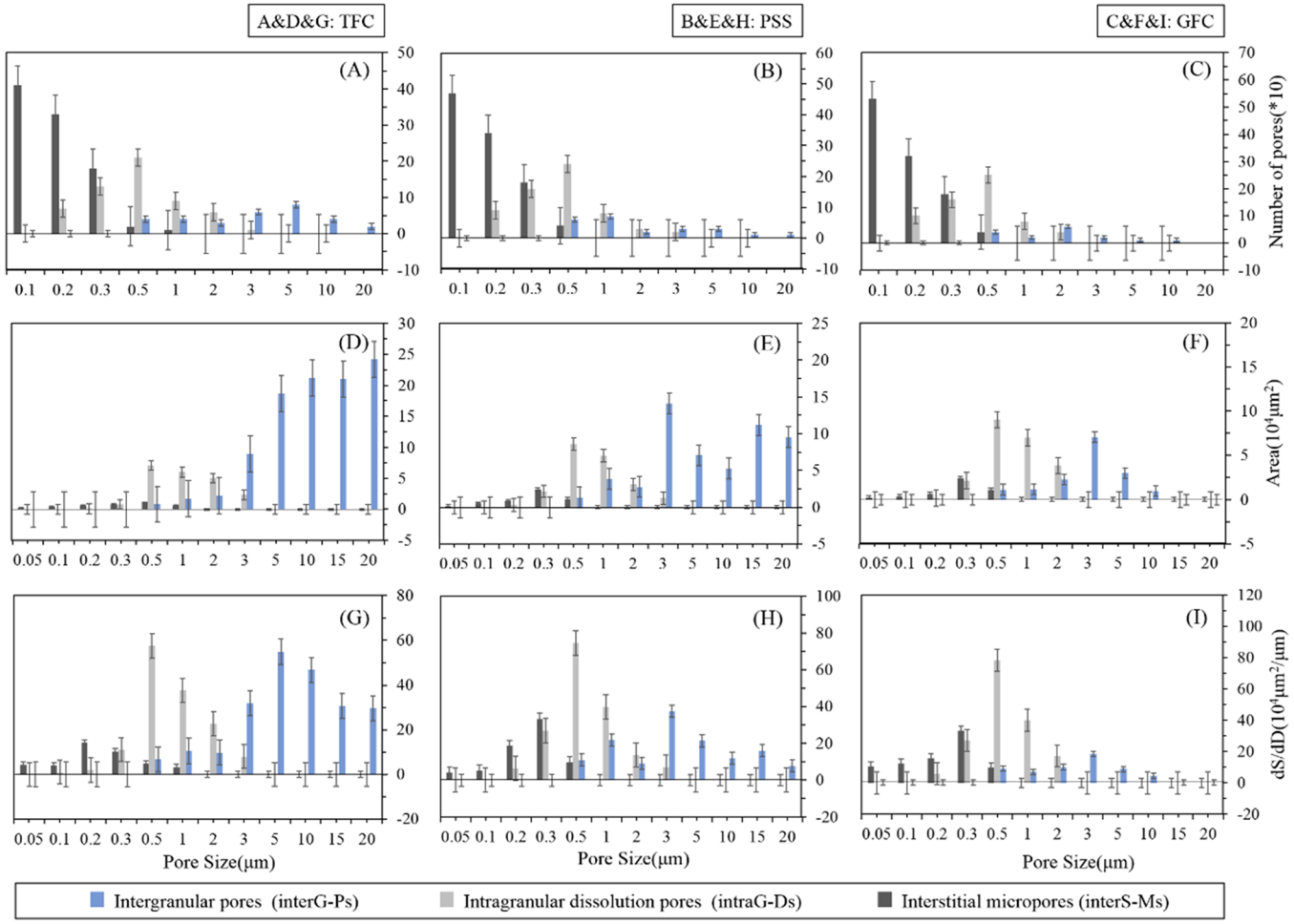

Figure 5. Microscopic pore characteristics of the three lithofacies. Panels (A−C) are the number distribution of different types of pores in traction flow conglomerate, pebbled sandstone, and gravity flow conglomerate. Panes (D−F) are the pore area distribution, and panels (G−I) are the d*S*/d*D*. The intergranular pores (interG-Ps) are more than 1 μm, the intragranular dissolved pores (intraG-Ds) are mainly 0.4−4 μm, and the interstitial micropores (interS-Ms) are mostly small pores below 1 μm. The main pore types of TFC and PSS are intergranular pores followed by intragranular dissolved pores. GFC contains a large number of intragranular dissolved pores and interstitial micropores

Different sizes of pores have divergent ability to allow fluids to pass through and have different contributions to permeability. According to the HPMI-NMR total pore distribution, the permeability contribution of pores of different sizes can be obtained. As shown in Figure 7, the pore with a cumulative permeability contribution of 95% is called the main flowing pore, and its average radius is called the main flowing pore radius (Rz), and the pore radius when the cumulative contribution of permeability is 99.9% is called the difficult-flowing pore radius (Rn). The main flowing pores represent well-connected pores; the pores between Rz and Rn provide most of the porosity, but the connectivity is inferior; in the pores below Rn, it is difficult for the nonwetting phase to displace the wetting phase, and the fluid is tough to flow. The Rz of sample T-3 is 2.81 μm, which only accounts for 5.8% of the total pore volume, but its contribution to permeability is as high as 66%. The Rn of sample is 0.032 μm, which contributes only 0.5% to permeability but occupies 42% of the pore volume.

4.5. Centrifugal Movable Fluid Analysis. NMR-centrifugal experiments can obtain abundant parameters such as movable pore cutoff (T2cutoff) and movable fluid saturation (MFS). In this study, the method of Zheng et al.[50] was used to determine the key pore size parameter T2cutoff. The steps are as follows: (1) Draw the cumulative pore diameter distribution curves of the core after saturation and centrifugation, respectively. (2) Make a parallel line from the highest point of the centrifugal cumulative curve and compare the saturation cumulative curve to a point. (3) The vertical line from the focus intersects the abscissa at a point, and the reading at this point is called the T2cutoff. The movable fluids of 12 typical samples were tested. T2cutoff was between 0.059 and 1.36 μm, with an average of 0.48 μm; MFS was between 9.24 and 41.38%, with an average of 23.35%. The MFS of TFC is 29.35−34.09%, with an average of 31.57%, which is relatively high overall; the lithology of different support structures in PSS differs significantly in movable fluid, the average MFS of P(G)SS is 33.28%, which is close to TFC, and the average MFS of P(F)SS is only 18.36%; GFC has the lowest movable fluid content, with a distribution range of 9.24−14.82%, with an average of 11.42%.

5. DISCUSSION

5.1. Impact of Sedimentation and Diagenesis on Reservoir Quality. Generally speaking, the factors affecting the physical properties of clastic reservoirs are divided into sedimentary factors and diagenetic alteration factors, and the sedimentary mechanism plays a dominant role.[5] The petrological characteristics of conglomerates, such as shaliness, clastic

https://doi.org/10.1021/acsomega.1c02952
ACS Omega 2021, 6, 23243−23261

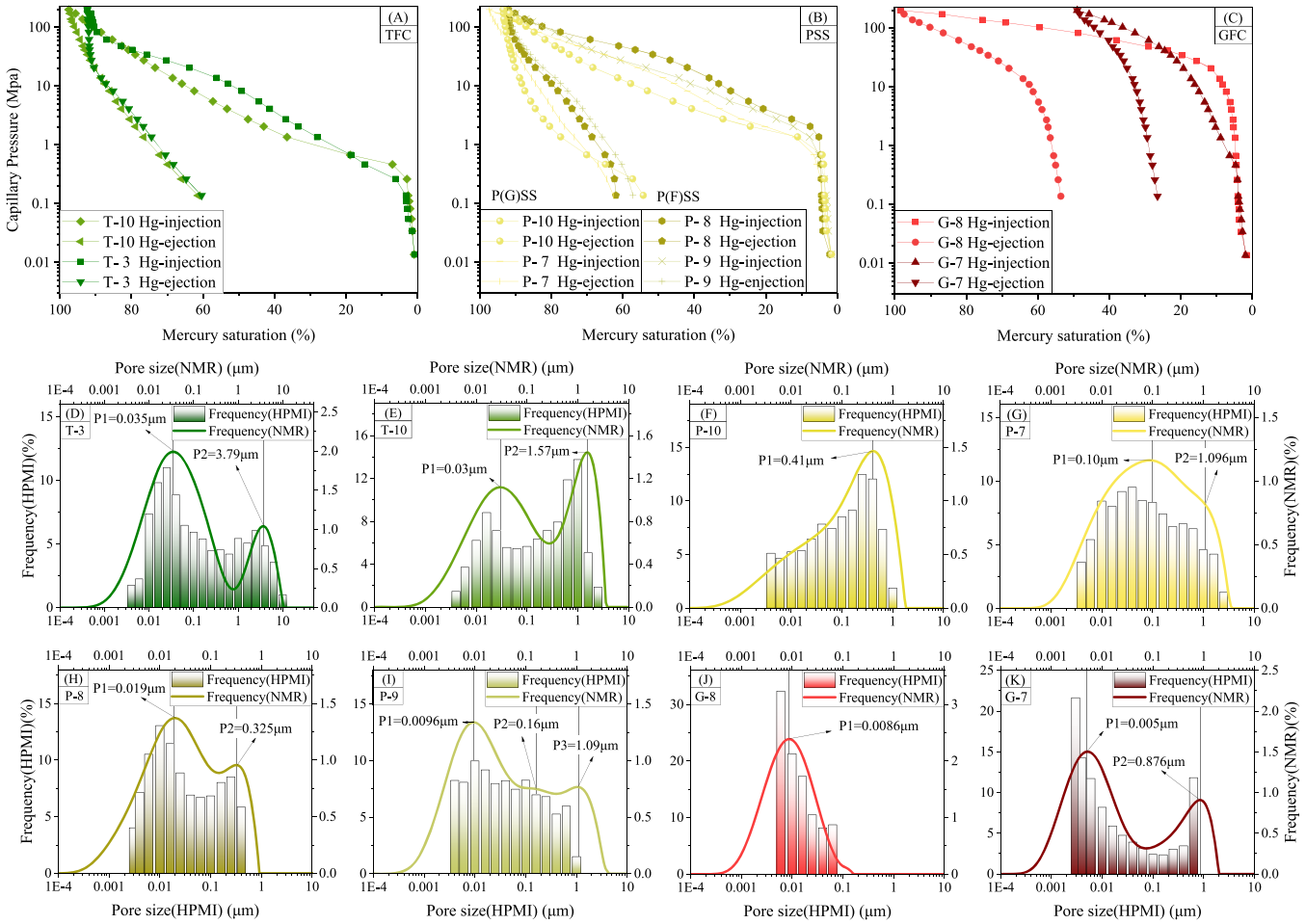

Figure 6. HPMI-NMR pore characteristics of three typical lithofacies samples in the Mahu conglomerate reservoir. Panels (A−C) are the capillary pressure curve of the three lithofacies, panels (D−K) are the pore size distribution of HPMI, pore size distribution of NMR after HPMI scale, and pore size peak position of the three lithofacies, respectively. The mercury intrusion threshold pressure of TFC, PSS, and GFC increased in turn, and the pore throat became smaller in turn. The distribution of TFC pore throat is mainly bimodal, P(G)SS is a mainly flat peak or single peak formed by a large pore, P(F)SS is mainly bimodal showing distinct smaller slanting degrees, and GFC is mainly single peak formed by a small hole.

composition, and particle distribution, are internal factors that affect the quality of its reservoir; diagenesis such as compaction and cementation is external factors. Different lithofacies have different comprehensive effects. The performance of reservoir quality varies significantly.

The oil-bearing reservoirs in the study area are generally coarser and poorly sorted. The shaliness and the clastic content have the closest relationship with the quality of the reservoir. The clastic content has an indirect effect on the quality of the reservoir by affecting compaction, dissolution, and other effects, which will be discussed in the next paragraph. The argillaceous is the clastic material with a particle diameter less than 0.01 mm, and it occupies the reservoir space and reduces the ability to resist compaction. At the same time, the clay minerals swell and migrate by absorbing water and block the pores. These are the decisive factors leading to the difference in the quality of conglomerate reservoirs with different depositional genes. Shaliness refers to the proportion of the volume of argillaceous to the total volume of the rock, and the specific value of shaliness was determined by casting thin section analysis in this study. The experimental results show that the shaliness has an exponentially declining relationship with permeability and a linearly declining relationship with porosity (Figure 8). TFC is under strong hydrodynamic conditions, its shale component content is washed out by mechanical differentiation, and the shaliness is mostly less than 3%; GFC is formed by the overall transportation of gravity flow without mechanical differentiation, and the content of PSS is mostly higher than 6%. The distribution of shaliness of PSS is quite different, P(G)SS is supported by coarse-grained miscellaneous particles, the water flow is full of washing effect, and the shaliness is less; P(F)SS is mostly supported by sandy shale, and the shale cementation is strong in the later stage. The mud content is higher.

Compaction is the main diagenetic pore reduction in the study area.[4] According to the pore parameter data under the mirror, the axial ratio, pore shape factor, and intensity factor are used to characterize the compaction effect. The pore shape factor (Fs) is the ratio of the actual area of the pore to the square of the perimeter, the pore intensity factor (Fi) is the ratio of the actual area of the pore to the area of the convex hull, and the axial ratio is the ratio of the major and minor axes of the ellipse circumscribed by the pore. The stronger the compaction effect, the smaller the value of Fs and Fi[51] and the larger the axial ratio. Figure 9 D,E shows that the Fs and Fi of the Mahu Sag reservoir are mainly distributed between 0.001−0.065 and 0.2−1,and as Fi decreases, compaction increases, Fs gradually decreases, and pore tortuosity increases, which may be related to pore boundary dissolution during compaction. Figure 9A−C shows

https://doi.org/10.1021/acsomega.1c02952
ACS Omega 2021, 6, 23243−23261

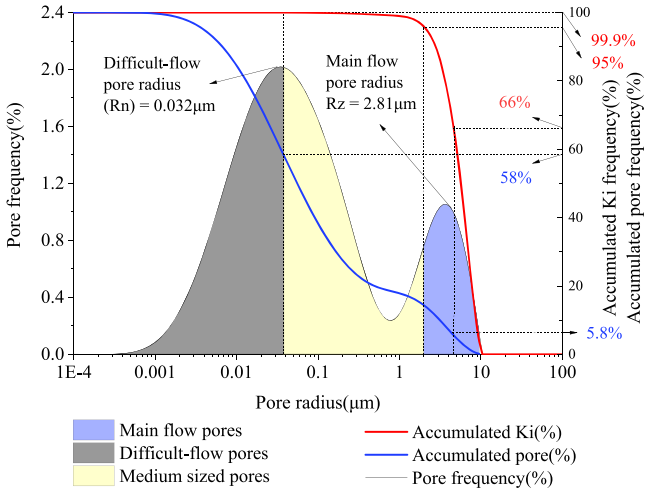

Figure 7. Schematic diagram for calculation of permeability contribution and main flow radius Rz and difficult-flow radius Rn of sample T-3. When the cumulative permeability contribution value reaches 95%, the pore is called the main flowing pore, and its mean radius is called the main flowing pore radius Rz. When the cumulative permeability contribution value reaches 99.9%, the corresponding pore radius is called the difficult flowing pore radius Rn

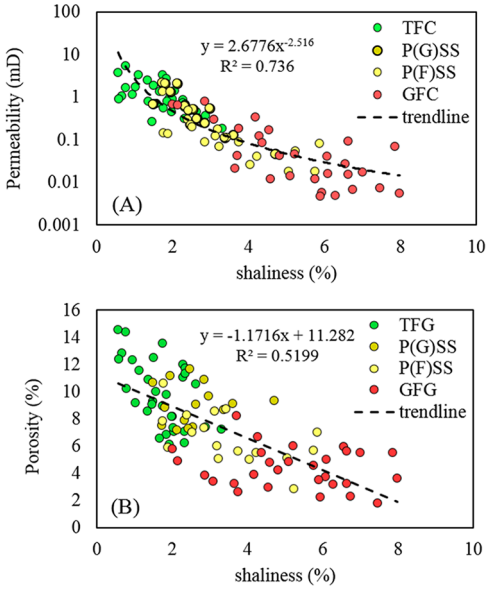

Figure 8. Relationship between shaliness and physical properties of three lithofacies. Panel (A) is the cross plot of shaliness and permeability.; Panel (B) is the cross plot of shaliness and porosity. The shale content has an exponentially decreasing relationship with permeability and a linearly decreasing relationship with porosity, which is an important factor controlling reservoir physical properties.

that, for the samples of the same lithofacies, the larger the pore size, the more high-axis ratio pores and the less low-axis ratio pores, indicating that compaction has a greater impact on interG-Ps and other macropores, while the supporting effect of rigid particles such as quartz inhibits the compaction of small pores such as dissolved pores in the grain. For samples of different lithofacies, TFC has high rigid particle content and low hetero-base content; the early precipitation of chlorite and zeolite minerals resisted normal compaction and at the same time provided flow space for acidic fluid dissolution in the middle diagenesis stage, resulting in weak pore compression but obvious dissolution at the edge of the pore; therefore, the Fi is generally higher, and the pore content with high axial ratio is the least, but the Fs is not high, and the reservoir quality is good; PSS is mostly located at the top of the traction flow sedimentary facies belt. Later diagenesis, such as infiltration and erosion, results in different effects of compaction and dissolution of PSS with different sand types and supporting structures; the Fs and Fi ranges are wider, and the high axial ratio pore content is higher; the shaliness of GFC is high, and the content of volcanic rock fragments is generally higher than 70%. At this time, the compaction rate is accelerated due to the internal defects or uneven structure of the fragments, the compaction reduction effect is the strongest, and its main pore types are dissolved pores and interstitial micropores, resulting in lower Fs and Fi, and the highest content of high axial ratio pores, pores with an axial ratio greater than 5, accounts for more than 60%, and the quality of the reservoir is inferior.

5.2. Influence of Pore Structure on Permeability. In this section, the HPMI-NMR experimental data of 32 cores are mainly used to analyze the influence of pore characteristic parameters on permeability in cores with different lithofacies.

Typical pore size parameters include average pore size (Rp), maximum pore size (Ra), main flow pore size (Rz), difficult-flow pore size (Rn), and so on (Table 1). Their relationship with permeability is shown in Figure 10A−D. According to the capillary model, permeability is often measured by the quadratic power of the average pore diameter. As can be seen from Figure 10A, the square of the average pore diameter of the three lithofacies is positively correlated with permeability, but the correlation is not obvious, which may be due to the complex pore throat structure and strong heterogeneity of conglomerate sandstone, which is greatly different from the capillary model. Permeability has a good linear correlation with the main flow radius, which may be because this parameter reflects the major contribution of the connected network composed of a large pore to the seepage flow. Permeability of TFC and PSS has a poor correlation with the maximum pore, but GFC has a good correlation, probably because GFC has a high shaliness and compact cement, the seepage flow mainly depends on the connected channels composed of a few largest pore throats. GFC and PSS are weakly positively correlated with difficult-to-flow pores, but TFC is negatively correlated with them, indicating that for high-quality reservoirs with good circulation networks, the cutoff effect of narrow throats has a greater impact on permeability.

The homogeneity coefficient α, the structure coefficient Φ_p, the sorting coefficient Sp, and the characteristic structure coefficient $1/D\Phi_p$ are the key parameters to measure the quality of the pore structure (Table 1). Their relationship with permeability is shown in Figure 10E−H. The homogeneity coefficient characterizes the deviation degree of each pore from the largest pore, and the permeability is negatively correlated with the homogeneity coefficient, indicating that small pores in homogeneous conglomerate reservoirs have a more restrictive effect on permeability than in heterogeneous reservoirs. The permeability has a more significant negative correlation with the structure coefficient, which indicates that the greater the difference between the actual pore and the ideal capillary model, the lower the permeability. In other words, the nonlinear resistance of fluid flow in the complex pore is also a significant factor affecting the permeability of conglomerate sandstone. The permeability of the three lithofacies is positively correlated with the sorting coefficient, and the correlation of GFC is more

https://doi.org/10.1021/acsomega.1c02952
ACS Omega 2021, 6, 23243−23261

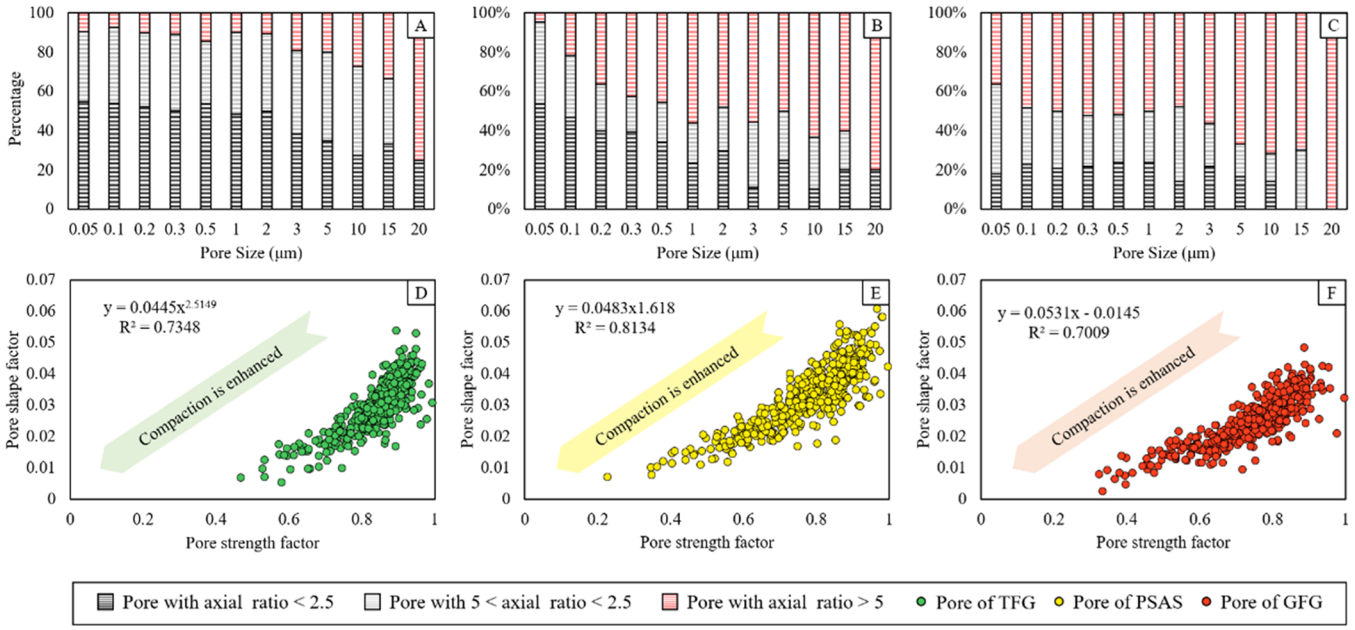

Figure 9. Characterization of compaction and pore reduction of three lithofacies in the Mahu conglomerate reservoir. (A) Facial ratios of pores with different axial ratios of TFC. (B) Facial ratios of pores with different axial ratios of PSS. (C) Facial ratios of pores with different axial ratios of GFC. (D) FS and Fi distribution of pores in TFC. (E) FS and Fi distribution of pores in PSAS. (F) FS and Fi distribution of pores in GFC. The average pore axis ratios of THC, PSS, and GFC are 3.04, 3.98, and 8.78; the average pore strength factors are 0.78, 0.77, and 0.74; and the average pore shape factors are 0.031, 0.033, and 0.024, respectively. The pore axis of conglomerates deposited by gravity flow is relatively large, and the average pore shape factor and pore strength factor are small, reflecting the strong action of compaction and dissolution, narrow pore throat structure, and poor reservoir quality. In addition, the larger the pore size is, the higher the high axial ratio porosity content is, indicating that the intergranular pores with larger pore sizes are easier to be compacted.

obvious, indicating that the sorting of pores is an important factor restricting the permeability of the GFC reservoir with poor sorting. For TFC and PSS caused by traction flow, the characteristic structural coefficients reflecting sorting and connectivity have a better positive correlation with permeability, which may be because hydrodynamic elutriation sometimes ignores narrow throats and forms local muddy blockages, leading to the more significant impact of connectivity on permeability.

5.3. Influence of Pore Types on Movable Fluid. The mobility of fluids in different types of pores is diverse. In previous studies, the influence of pore types on movable fluids was often not well quantified, and HPMI-NMR alone could not effectively distinguish pore types. Therefore, this study adopted the idea of linear spectral decomposition (LSD).[35,52,53] The total pore size distribution of HPMI-NMR is approximately considered to be a linear combination of the probability distribution of different types of pore sizes:

$$y(r) = \sum_{i=1}^{n} f_i x_i(r) \tag{1}$$

$$s.\ t.\ \sum_{i=1}^{n} f_1 = 1,\ f_i \geq 0 \tag{2}$$

In the formula, n is the number of pore types, $x_i(r)$ is the PSD of the ith pore, and f_i is the proportion of space occupied by the ith pore. At the same time, non-negative constraints are used to ensure that the sum of the scores is 1, and the problem is expressed as a matrix:

$$Y = XF + e \tag{3}$$

where X is the PSD matrix of different pores and e is the error vector that must be minimized in order to obtain the most suitable F. According to the PSD of different types of pores obtained from the mirror image and the PSD before and after centrifugation described by HPMI-NMR in Section 4. We use the least squares solution to solve this problem:

$$F = (X^{\mathrm{T}}X)^{-1}X^{\mathrm{T}}Y \tag{4}$$

Based on this, we can estimate the proportion of each type of pore in different samples before and after centrifugation and quantify the fluid mobility in various types of pores so as to further analyze the movable fluid characteristics of different lithofacies samples.

Figure 11 is a schematic diagram of movable fluids in different types of pores of six typical samples with three lithofacies. Overall, the MFS of interG-Ps is 39.22−91.47%, with an average of 65.43%; that of intraG-Ds is 19.60−53.78%, with an average of 35.70%; and that of interS-Ms is 3.87−26.31%, with an average of 9.20%. As can be seen, interG-Ps contribute significantly to fluid mobility and provide the primary flow channel, while interS-Ms and intraG-Ds contribute less to the formation of an effective percolation network. Specific analysis of six typical samples was done. It can be seen from Figure 11, groups A and B, that the movable fluid saturation of the TFC sample is overall higher, above 30%, mainly due to the bimodal pore size distribution, and the hard particles support a large amount of interG-Ps, and the fluid in the pores is highly mobile. At the same time, it can be seen that the movable fluid saturation of the micropores such as interS-Ms of the two samples is also higher than that of the other samples, indicating that a good seepage network composed of intergranular pores is also beneficial to improve the fluid mobility of the micropores. PSS

https://doi.org/10.1021/acsomega.1c02952
ACS Omega 2021, 6, 23243−23261

Table 1. Lithology, Physical Properties, and Pore Structural Parameters of Conglomerate Samples of Three Sedimentary Lithofacies[a]

sample types	sample no.	well	formation	lithology	lithofacies	helium porosity (%)	permeability (mD)	oiliness	shaliness	Rp	Rz	Ra	Rn	α	Φp	Sp	$1/D\Phi_p$
type 1	T-1	M027	Baikouquan	gray glutenite	TFG	10.89	0.244	fluorescence	1.47	0.313	1.83	5.703	0.16	0.22	0.947	0.698	0.04
	T-2	M027	Baikouquan	gray glutenite	TFG	11.58	3.306	oil spot	1.85	1.511	7.66	11.336	0.09	0.151	0.102	1.751	0.947
	T-3	M027	Baikouquan	green-gray glutenite	TFG	8.58	2.447	oil spot	1.34	0.397	2.81	9.624	0.032	0.141	0.069	0.826	0.695
	T-4	M027	Baikouquan	green-gray glutenite	TFG	9.19	1.681	oil spot	1.03	0.207	5.9	8.583	0.013	0.256	0.029	0.654	1.559
	T-5	M027	Baikouquan	green-gray glutenite	TFG	6.58	1.349	oil spot	1.66	0.459	3.13	6.108	0.11	0.3	0.128	0.956	0.374
	T-6	M027	Baikouquan	gray glutenite	TFG	13.58	0.551	fluorescence	1.75	1.333	4.12	13.006	0.32	0.318	3.289	1.481	0.017
	T-7	M027	Baikouquan	green-gray glutenite	TFG	8.18	0.41	fluorescence	2.64	0.684	3.41	8.04	0.16	0.34	1.167	1.242	0.047
	T-8	M027	Baikouquan	green-gray glutenite	TFG	14.54	3.739	oil stains	0.57	1.723	8.452	10.881	0.081	0.233	0.109	1.907	0.836
	T-9	K206	Wuerhe	gray glutenite	TFG	11.04	0.845	oil immersion	2.28	0.694	2.718	7.054	0.126	0.393	0.786	1.218	0.072
	T-10	K207	Wuerhe	gray glutenite	TFG	12.37	0.893	oil immersion	0.59	0.528	1.965	5.749	0.235	0.367	0.482	0.764	0.143
	T-11	M027	Baikouquan	green-gray glutenite	TFG	7.36	0.644	oil spot	2.03	1.338	4.888	11.411	0.306	0.369	0.311	2.138	0.201
	T-12	M027	Wuerhe	gray glutenite	TFG	11.23	0.67	oil spot	1.49	0.112	0.7	1.024	0.019	0.439	0.265	0.188	0.296
	average					10.43	1.4		1.56	0.775	3.965	8.21	0.138	0.294	0.64	1.152	0.436
type 2	P-1	K206	Wuerhe	gray pebbly fine sandstone	P(F)SS	2.85	0.053	oil stains	5.21	0.486	2.07	3.525	0.122	0.494	1.276	0.732	0.047
	P-2	K206	Wuerhe	gray pebbly fine sandstone	P(F)SS	8.59	0.122	fluorescence	3.13	0.428	3.22	8.06	0.78	0.289	4.664	2.038	0.013
	P-3	K206	Wuerhe	gray pebbly fine sandstone	P(F)SS	5.02	0.026	oil immersion	4.04	0.215	1.231	2.179	0.047	0.395	1.12	0.362	0.053
	P-4	K206	Wuerhe	pebbled gritty sandstone	P(G)SS	8.84	2.085	oil immersion	1.81	0.652	4.908	7.543	0.131	0.358	0.182	1.737	0.338
	P-5	M032	Wuerhe	pebbled gritty sandstone	P(G)SS	7.88	1.22	oil immersion	1.95	0.34	6.134	13.006	0.107	0.105	0.093	0.932	0.391
	P-6	K206	Wuerhe	gray pebbly fine sandstone	P(F)SS	5.53	0.01	oil spot	5.05	0.312	1.441	4.024	0.066	0.494	3.101	0.364	0.017
	P-7	M18	Wuerhe	maroon isometric sandstone	P(G)SS	5.9	1.52	fluorescence	1.74	0.278	1.296	3.291	0.061	0.338	0.134	0.485	0.427
	P-8	M027	Baikouquan	gray pebbly fine sandstone	P(F)SS	5.15	0.0177	oil stains	5.75	0.104	0.46	0.912	0.072	0.314	0.893	0.414	0.05
	P-9	M027	Baikouquan	gray pebbly fine sandstone	P(F)SS	7.04	0.096	oil stains	5.86	0.291	2.352	4.64	0.098	0.343	0.906	0.571	0.077
	P-10	M027	Wuerhe	maroon isometric sandstone	P(G)SS	8.68	0.111	fluorescence	3.43	0.282	1.256	1.71	0.124	0.265	0.776	1.074	0.118
	average					6.55	0.53		3.797	0.339	2.437	4.889	0.161	0.340	1.315	0.871	0.153
type 3	G-1	M027	Wuerhe	gray conglomerate	GFG	3.93	0.0057	fluorescence	5.94	0.05	0.732	0.432	0.034	0.478	0.867	0.18	0.064
	G-2	M027	Wuerhe	gray conglomerate	GFG	4.22	0.0429	fluorescence	4.81	0.141	0.81	1.546	0.027	0.364	0.244	0.241	0.239
	G-3	M027	Wuerhe	gray conglomerate	GFG	5.82	0.681	fluorescence	2	0.202	2.9	4.978	0.046	0.214	0.044	0.71	2.23
	G-4	M027	Wuerhe	gray glutenite	GFG	5.67	0.121	oil stains	4.28	0.069	0.346	0.678	0.014	0.406	0.028	0.098	2.525
	G-5	M027	Wuerhe	gray conglomerate	GFG	2.9	0.301	oil stains	3.1	0.261	1.871	3.291	0.066	0.317	0.082	0.493	0.945
	G-6	M027	Wuerhe	maroon glutenite	GFG	5.96	0.027	fluorescence	6.55	0.057	0.227	0.419	0.01	0.549	0.091	0.072	0.87
	G-7	M027	Wuerhe	gray conglomerate	GFG	8.26	0.0421	oil spot	3.71	0.197	1.03	1.895	0.125	0.104	0.05	0.365	1.589
	G-8	M027	Wuerhe	maroon	GFG	3.87	0.799	fluorescence	2.86	0.093	0.076	0.186	0.032	0.188	0.031	0.128	1.318
	G-9	M027	Wuerhe	gray glutenite	GFG	4.99	0.016	oil stains	6.1	0.065	0.126	0.615	0.008	0.425	0.115	0.093	0.61
	G-10	M027	Wuerhe	maroon glutenite	GFG	5.51	0.084	fluorescence	4.37	0.127	1.06	3.191	0.025	0.159	0.132	0.394	0.244

https://doi.org/10.1021/acsomega.1c02952
ACS Omega 2021, 6, 23243−23261

Table 1. continued

sample types	sample no.	well	formation	lithology	lithofacies	helium porosity (%)	permeability (mD)	oiliness	shaliness	Rp	Rz	Ra	Rn	α	Φp	Sp	$1/D\Phi_p$
	average					5.11	0.21		4.37	0.126	0.918	1.723	0.039	0.320	0.168	0.277	1.063

[a]Rp is mean radius; Rz is main flow radius; Ra is the maximum radius; Rn is the difficult-flow pore size; α is homogeneity coefficient; Φ_p is the structure coefficient; Sp is sorting coefficient; $1/D\Phi_p$ is the characteristic structure coefficient.

sample characteristics have obvious difference and can be divided into two categories, such as that shown in Figure 11, group C, its lithology is pebbled gritty sandstone, multistage coarse sand support, shaliness is low, it has better properties, the distribution of pore is a flat peak shape distribution, and each kind of pore of MFS is higher; the other one, as shown in Figure 11, group D, a lithology of pebbled fine sandstone, the gravel is filled with a silty matrix, the gravel is floating, with high argillaceous content, bimodal showing skewness with smaller slanting degrees in pore distribution, low content of interG-Ps, and low MFS. There are individual samples in GFC as shown in Figure 11, group F. There is a small amount of discontinuous storage space around 1 μm, mainly due to the high content of impurities in the gravity flow sedimentation, weak shale cementation strength, and easy-to-produce interfacial cracks. The fluid is easily discharged. However, most GFCs are shown in Figure 11, group E. The pore types are mainly intraG-Ds and interS-Ms, and MFS is less, mostly around 15%.

5.4. Geological Control of Fluid Mobility. Geological controlling factors, such as deposition and diagenesis, have an important influence on fluid mobility. The conglomerates in different sedimentary environments have different mineral compositions and different diagenetic effects such as compaction and cementation, which further lead to differences in fluid mobility.

Sedimentation affects the mineral composition of the conglomerate, which in turn affects the fluid mobility. The type and content of clay minerals have an important impact on the fluid mobility. It can be seen from Figure 12A−D that the saturation of the movable fluid is obviously negatively correlated with the total amount of clay minerals. Among them, the content of I/S is strongly negatively correlated with the movable fluid saturation, mainly because I/S develops in a large amount of silk hair, and it is easy to swell with water to block pores and throats, reducing fluid mobility. According to the I/S content, the samples can be divided into two categories: traction flow conglomerates and pebbled gritty sandstone are low I/S content (15−55%) conglomerates, and the movable fluid saturation is higher. The I/S content of gravity flow conglomerates and pebbly fine sandstone is relatively high (75−95%), and the saturation of movable fluid is low; other clay minerals such as illite and kaolinite have relatively little influence on fluid mobility; illite mainly adheres to the particle surface and throat to reduce the pore connectivity, while kaolinite and chlorite mainly surround the particle surface to reduce the pore volume, and its content has a weak negative correlation with the saturation of the movable fluid.

Diagenesis such as compaction and cementation has an important influence on fluid mobility, and its effect is closely related to the mineral composition. Figure 12E,F shows that there is a strong positive correlation between the content of quartz and feldspar and the saturation of the movable fluid. The main reason is that the higher the content of rigid particles such as quartz and feldspar, the stronger the compaction resistance of the rock, which is more conducive to the preservation of primary intergranular pores. Intergranular pores are the type of pores with the strongest fluid mobility. The dissolution pores that developed in the feldspar are beneficial to improve the seepage network and enhance fluid mobility. The compaction rate and cementation rate of the experimental core can be obtained through rock slices. The compaction rate refers to the proportion of the volume other than the intergranular volume to the original pore volume, and the cementation rate refers to

https://doi.org/10.1021/acsomega.1c02952
ACS Omega 2021, 6, 23243−23261

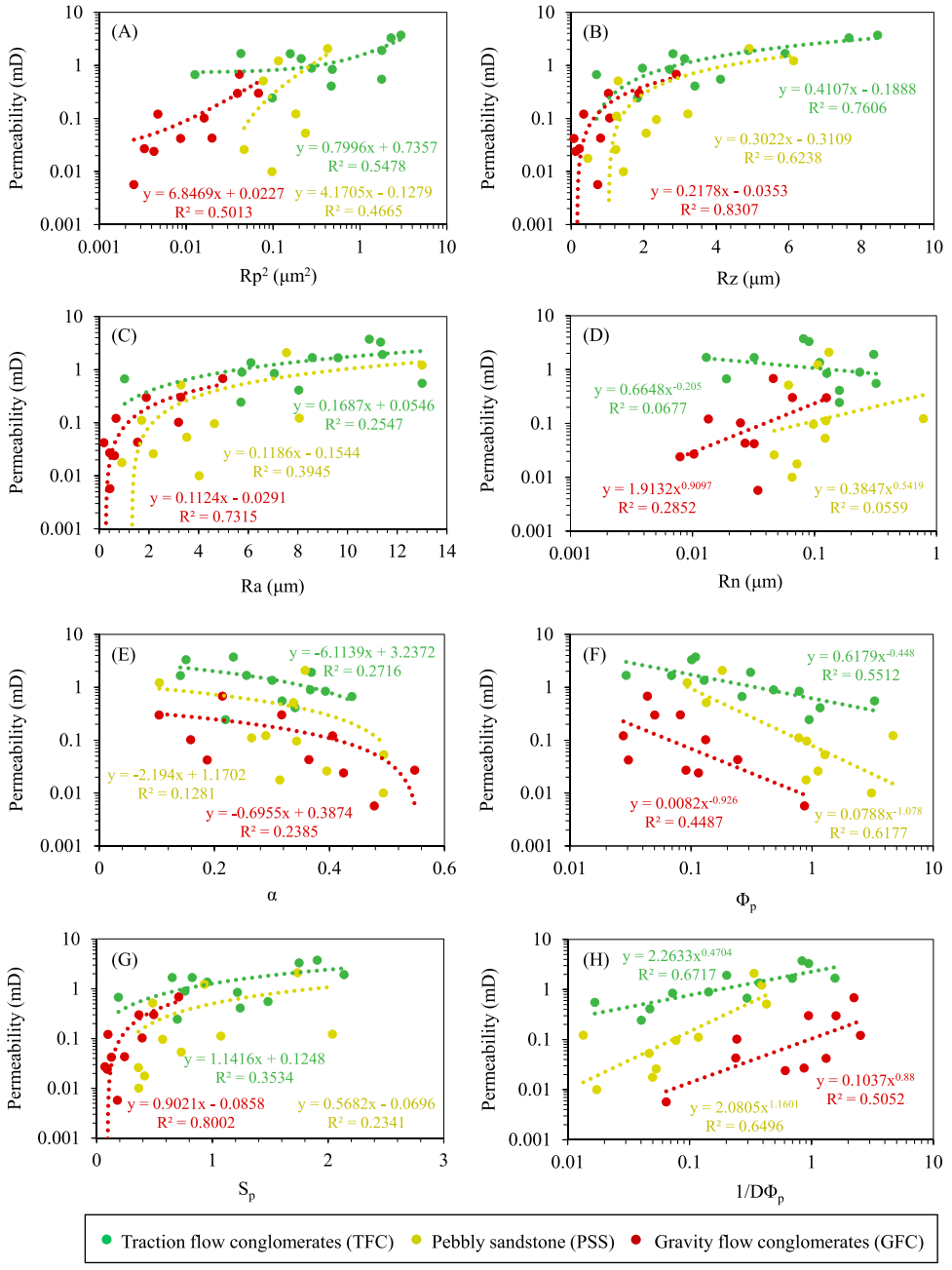

Figure 10. Correlation between key pore size parameters, pore characteristic parameters, and permeability. It mainly includes the (A) square of mean radius R_P^2, (B) main flow radius Rz, (C) maximum radius Ra, (D) difficult-flow pore size Rn, (E) homogeneity coefficient α, (F) structure coefficient Φ_p, (G) sorting coefficient SP, (H) and characteristic structure coefficient $1/D\Phi_p$. The permeability of conglomerate sandstone is positively correlated with the square of mean radius R_P^2, the main flow radius Rz, the maximum radius Ra, the sorting coefficient Sp, and the characteristic structure coefficient $1/D\Phi_p$ and negatively correlated with the homogeneity coefficient α and the structure coefficient Φ_p. The permeability of GFC is more dependent on the maximum pore size and the size of sorting, while the permeability of TFC is more affected by the connectivity. Compared with other pore size parameters, the main flow radius Rz can better describe the reservoir permeability.

the proportion of the cement volume to the original pore volume, which respectively represent the degree of compaction and cementation. It can be seen from Figure 12G,H that the compaction rate is negatively correlated with the movable fluid saturation, indicating that compaction causes the effective storage space to decrease, and the movable fluid saturation decreases. The cementation rate is positively correlated with the saturation of the movable fluid, mainly because the cement can hinder the compaction from destroying the pores to a certain extent. At the same time, the cement occurs in the dominant channel of the large pores, which can increase the swept area of fluid flow and make the saturation of the movable fluid increase.

Wettability is another important geological control parameter, which has an important influence on the flow and occurrence of fluid in the core. The movable fluid experiment was carried out on two traction flow conglomerate cores in the original wet state without oil washing. The core washed with petroleum ether can be considered to be in a strong water wet state, while the core in the original state can be considered to be in an oil wet or weak oil wet state, the comparison between the two can be used to obtain the influence of wettability on fluid mobility. From the

https://doi.org/10.1021/acsomega.1c02952
ACS Omega 2021, 6, 23243−23261

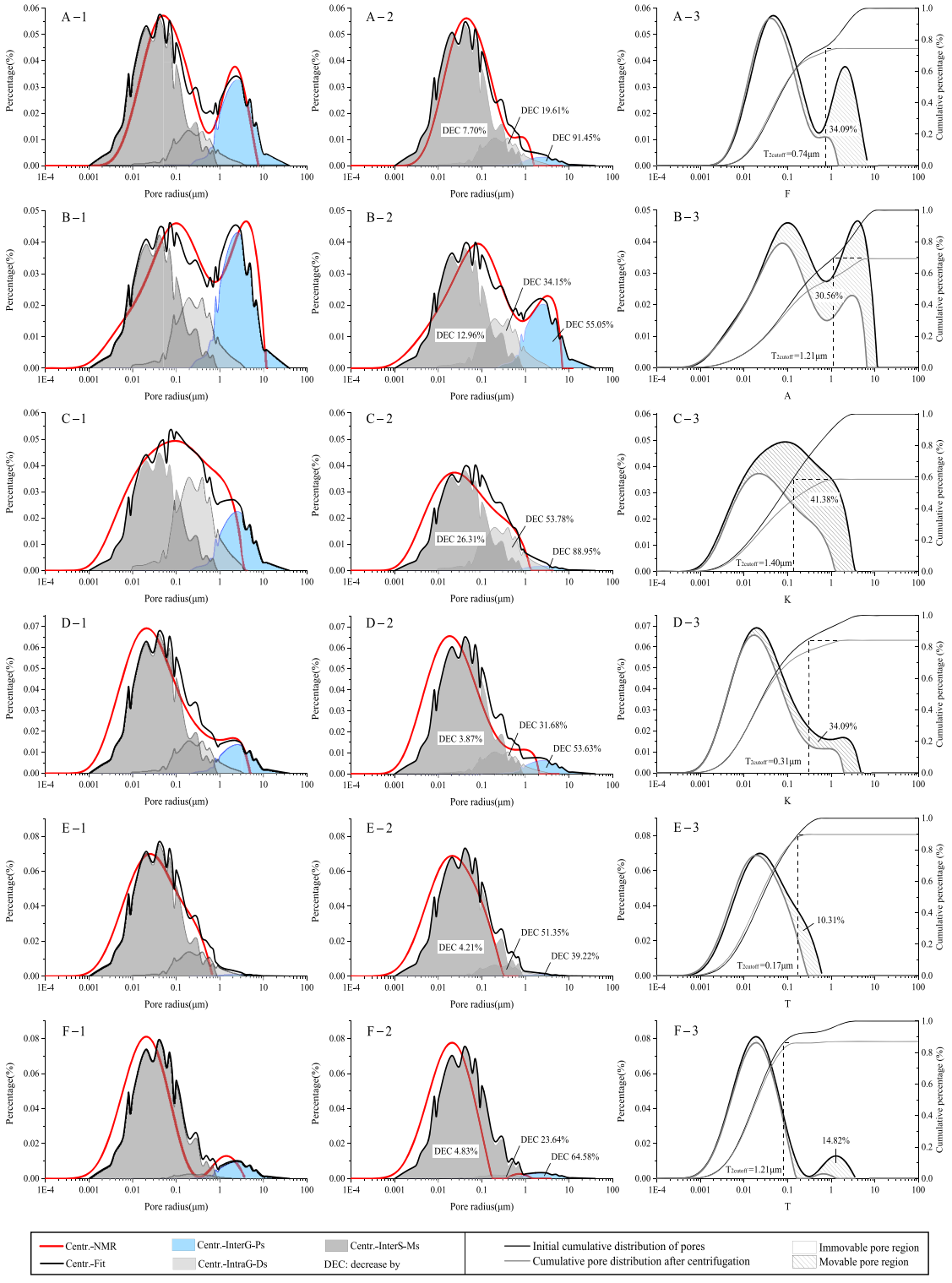

Figure 11. Movable fluid, total movable fluid, and T2cutoff of different types of pores in six typical samples of three lithofacies. This includes the following: (group A) sample T-9, (group B) sample T-11, (group C) sample P-7, (group D) sample P-6, (group E) sample G-9, and (group F) sample G-10. The average movable fluid saturation of intergranular pores, intragranular dissolved pores, and interfilling micropores are 65.43, 35.70, and 9.20%, respectively, and the fluid mobility in intergranular pores is the highest. The movable fluid saturation of TFC samples is high, but there are two types, the difference lies in the different distribution modes of clay minerals. P(F)SS and GFC samples have less intergranular pores and lower movable fluid saturation.

experimental results in Table 2, it can be seen that the movable fluid saturation of the core in the original state is higher than 35%, which is slightly higher than that of the traction flow conglomerate sample in the wet state. This is mainly because the hydrophilicity of the particle surface will increase the flow resistance of the water phase, and at the same time, more bound water will be formed in the small pores or capillaries, which will reduce the fluid mobility. In actual reservoirs, gravity flow

https://doi.org/10.1021/acsomega.1c02952
ACS Omega 2021, 6, 23243−23261

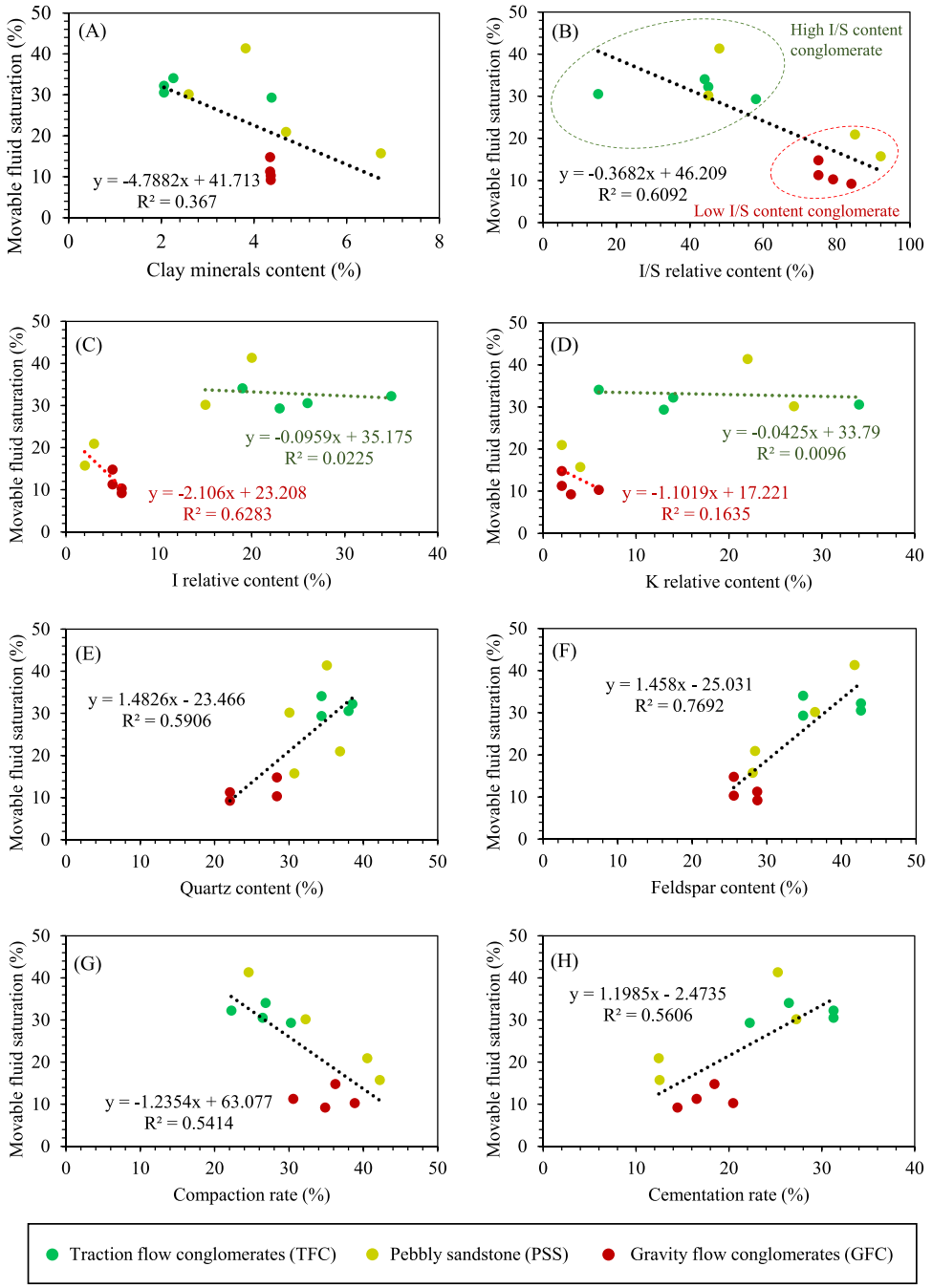

Figure 12. Relationship between moveable fluid saturation and mineral composition and diagenesis parameters. These include the (A–F) relationship between the content of clay minerals, I/S mixed layer, illite, kaolinite, quartz, feldspar, and movable fluid saturation. (G–H) Relation between the compaction rate, cementation rate, and moveable fluid saturation. The movable fluid saturation has a negative correlation with the content of clay minerals, especially the content of I/S, and a positive correlation with the content of hard particles such as quartz and feldspar. Compaction reduces fluid mobility, while cementation increases fluid mobility.

conglomerates have poor physical properties and oil-bearing properties and are more water-wet than traction flow conglomerates. The difference in wettability is an important factor in the fluid mobility of different lithofacies conglomerates.

5.5. Reservoir Quality Classification Based on Sedimentary Genesis and Supporting Structures. According to the muddy complex, pore structure, movable fluid, etc., the conglomerate reservoirs in the southern slope of Mahu are divided into two types: type I with favorable reservoirs and type II with nonfavorable reservoirs. The specific characteristic parameters are as follows (Table 3).

In type I, favorable reservoirs mainly include TFC and P(G)SS, which are blown in with multiple pressures after trial production. The daily test oil volume is 3–30 t. The lithology is small conglomerate, pebbled gritty sandstone, supported by multi-level particles and mixed base particles. The shaliness is mostly less than 4%, the clay mineral content is less than 3.8%, the relative content of the I/S mixed layer is less than 55%, the content of volcanic rock clastics is less than 60%, and the porosity and permeability are mostly above 6% and 0.1 mD. InterG-Ps and intraG-Ds are the main ones. The PSD curves of NMR are dominated by bimodal, unimodal, and flat peaks

https://doi.org/10.1021/acsomega.1c02952
ACS Omega 2021, 6, 23243–23261

Table 2. Movable Fluid and Clay Mineral Content of Conglomerate Samples of Three Sedimentary Facies[a]

sample types	sample no.	lithofacies	quartz (%)	feldspar (%)	clay mineral (%)	I/S (%)	I (%)	K (%)	MFS (%)	MFS of interG-Ps (%)	MFS of intraG-Ds (%)	MFS of interS-Ms (%)	wettability
type 1	T-13	TFC	33.42	40.12	2.35	22	32	26	38.45				original wet
	T-14	TFC	36.12	42.34	2.21	42	26	8	35.12				original wet
	average		34.77	41.23	2.28	32	29	17	36.785				
type 2	T-11	TFC	38.02	42.6	2.05	15	26	34	30.57	55.05	34.15	12.96	water wet
	T-4	TFC	38.53	42.6	2.06	45	35	14	32.25	65.2	30.36	10.86	water wet
	T-9	TFC	34.38	34.86	2.26	44	19	6	34.09	91.48	19.61	7.69	water wet
	T-12	TFC	34.38	34.86	4.38	58	23	13	29.36	76.43	14.32	11.25	water wet
	average		36.33	38.73	2.69	40.5	25.75	16.75	31.57	72.04	24.61	10.69	
type 3	P-4	P(G)SS	30.06	36.46	2.59	45	22	27	25.18	69.05	42.36	17.32	water wet
	P-7	P(G)SS	35.08	41.76	3.82	48	20	22	41.38	88.95	53.78	26.31	water wet
	P-6	P(F)SS	30.73	28.1	6.74	92	2	4	15.75	53.63	31.68	3.87	water wet
	P-3	P(F)SS	36.88	28.42	4.69	85	3	2	20.96	45.3	27.42	8.32	water wet
	average		33.19	33.69	4.46	67.5	11.75	13.75	25.82	64.23	38.81	13.96	
type 4	G-2	GFC	22.06	28.72	4.36	84	6	3	9.25	39.45	42.32	7.35	water wet
	G-1	GFC	22.06	28.7	4.35	75	5	2	11.3	41.16	34.01	10.35	water wet
	G-9	GFC	28.38	25.56	4.36	79	6	6	10.31	39.22	51.35	4.21	water wet
	G-10	GFC	28.38	25.56	4.35	75	5	2	14.82	64.58	23.64	4.83	water wet
	average		25.22	27.135	4.36	78.25	5.50	3.25	11.42	46.1	37.83	6.69	

[a]I/S is the illite/smectite mixed layer; I is illite; K is kaolinite; MFS is movable fluid saturation.

showing skewness with greater or slightly smaller slanting degrees. The permeability contribution is mainly provided by the micropores above 1 μm, the connectivity of the pore network has a great influence on seepage, the main flow radius is mostly higher than 1.5 μm, MFS is higher than 20%, and T2cutoff is mostly higher than 0.6 μm.

In type II, nonfavorable reservoirs are mainly GFC and P(F)SS. Trial production requires swabbing. The daily test oil volume is less than 5 t or there is no oil and gas display. The lithology is large and medium conglomerate, pebbly fine sandstone; the argillaceous and clay minerals are mostly higher than 4%, the content of I/S mixed layer is generally higher than 75%, the content of volcanic rock clastics is mostly higher than 75%, and the porosity and permeability are above 8% and 1 mD for the most part. The pore types are mainly intraG-Ds and interS-Ms. The PSD curves of NMR are mostly bimodal, unimodal, and multimodal with smaller slanting degrees. Submicron pores of 0.1−1 μm provide the main permeability contribution. The size of the macropores and sorting properties have a great influence on the seepage, the main flow radius is mostly less than 2 μm, the MFS is less than 20%, and the T2cutoff is less than 0.6 μm in most cases.

Reservoir quality classification is in good agreement with on-site oil testing. However, it is not possible to identify lithofacies based on the above differences in physical properties. Various lithofacies often appear alternately in the vertical direction in the form of sand layers. The research should start from the perspective of sedimentation; comprehensively judge the lithofacies according to the location, flood period, particle size probability curve, rock structure, etc.; and then proceed to evaluate the quality of the reservoir.

6. CONCLUSIONS

This paper mainly studies the physical properties of pores, movable fluids, and reservoir quality of the conglomerate reservoirs of the Wuerhe to Baikouquan Formation in the southern slope of the Mahu Depression. The conclusions are as follows:

(1) The study area mainly has three lithofacies: TFC, PSS, and GFC. PSS can be subdivided into P(G)SS and P(F)SS. TFC and P(G)SS that mostly contain small gravel and coarse sand, supported by multi-level grains and mixed base particles, with good oil content and trial production, are type I favorable reservoirs; GFC and P(F)SS that contain medium and large gravels and fine sand, supported by mixed base particles or matrix, belong to type II nonfavorable reservoirs.

(2) The shaliness and compaction are the key controlling factors affecting the physical properties of conglomerates. The shaliness decreases exponentially with permeability and linearly with porosity. A new parameter, the long-axis to short-axis ratio (axial ratio) of the pore outer ellipse, is proposed to quantitatively describe the compaction. The average axial ratios of the three lithofacies are 3.04, 3.98, and 8.78, respectively, and the compaction of the reaction is enhanced successively.

(3) According to HPMI and NMR, the influence of pore characteristics of the three lithofacies samples on permeability is analyzed. The permeability of conglomerate sandstone is positively correlated with the square of mean radius R_p^2, the main flow radius Rz, the maximum radius Ra, the sorting coefficient Sp, and the characteristic structure coefficient $1/D\Phi_p$ and negatively correlated with the homogeneity coefficient α and the structure coefficient Φ_p. The main controlling factors of permeability of GFC and TFC are sorting and connectivity, respectively, and the main flow radius Rz is the most suitable parameter to describe permeability.

(4) A linear spectral decomposition (LSD) method was used to establish a new quantitative calculation method of movable fluid saturation for different types of pores, the moveable fluid saturation values of intergranular pores, intragranular dissolved pores, and interfilling micropores are 65.43, 35.70, and 9.20%, respectively. Movable fluid saturation is inversely proportional to clay mineral content, especially I/S content, and is directly

https://doi.org/10.1021/acsomega.1c02952
ACS Omega 2021, 6, 23243−23261

Table 3. Reservoir Quality Classification Based on Sedimentary Genesis and Supporting Structure[a]

Reservoir levels	type I favorable reservoirs		type II non-favorable reservoirs	
Trial production (t/d)	3~30		<5	
Sedimentary facies	TFC	P(G)SS	P(F)SS	GFC
Deposition mechanism	tractive flow	tractive flow	tractive flow	gravity flow
sedimentary facies	Bottoms of offshore underwater distributary channels; below the wave base	Tops of offshore underwater distributary channels; underwater environment	the front mud debris flow and clastic flow deposits; Land environment	
	Bottoms of fan channels and inshore subaqueous distributary channels	The inter-river channel and tops of the inshore underwater distributary channel	The plain mud debris flow and clastic flow deposits	
lithology	Small conglomerate, fine conglomerate	Pebbled gritty sandstone	Pebbled fine sandstone	Large and medium-sized conglomerate
structural support	Multi-stage particle support, particle support	Heterobase-particle support	matrix-support	matrix-particle support
shaliness (%)	0~4	1~5	2~6	3~9
Volcanic clastics content (%)	<60		>75	
Clay mineral content (%)	1< total<4 I/S<55		2< total<7 I/S>75	
porosity (%)	>6	>5	4~10	<6
permeability (mD)	>0.1		0.01~1	<1
pore type	Mainly InterG - Ps, IntraG-Ds		Mainly IntraG-Ds, InterS-Ms	
Main flow pore (μm)	4~14		0.05~4	
The PSD form	bimodal, unimodal, and flat peaks showing skewness with greater or slightly smaller slanting degrees		bimodal, unimodal and multimodal with smaller slanting degrees	
sorting coefficient	0.5~2.5		<1	
Characteristic structure coefficient	0.01-1		0.1-5	
MFS (%)	>20		<20	
T2cutoff (μm)	0.5~1.5		<0.5	

[a]PSD is the pore size distribution.

proportional to the content of hard particles such as quartz and feldspar. Compaction is not conducive to fluid mobilization, and cementation is conducive to improving fluid mobility. The fluid mobility of water-wet samples is worse than that of oil-wet samples. TFC and P(G)SS contain more moveable fluid saturation than P(F)SS and GFC.

AUTHOR INFORMATION

Corresponding Author

Shenglai Yang − *State Key Laboratory of Petroleum Resources and Prospecting, China University of Petroleum (Beijing), Beijing 102249, China*; Phone: +86 13911918387; Email: ysltg2021@163.com

Authors

Jianbang Wu − *State Key Laboratory of Petroleum Resources and Prospecting, China University of Petroleum (Beijing), Beijing 102249, China*; orcid.org/0000-0002-6887-5335

Bowen Gan − *State Key Laboratory of Petroleum Resources and Prospecting, China University of Petroleum (Beijing), Beijing 102249, China*

Yushun Cao − *State Key Laboratory of Petroleum Resources and Prospecting, China University of Petroleum (Beijing), Beijing 102249, China*

Wei Zhou − *Experimental Test Research Institute of XinJiang Oilfield Company, Karamay 834000, China*

Gen Kou − *Experimental Test Research Institute of XinJiang Oilfield Company, Karamay 834000, China*

Ziqiang Wang − *Experimental Test Research Institute of XinJiang Oilfield Company, Karamay 834000, China*

Qiang Li − *State Key Laboratory of Petroleum Resources and Prospecting, China University of Petroleum (Beijing), Beijing 102249, China*

Wengang Dong − *State Key Laboratory of Petroleum Resources and Prospecting, China University of Petroleum (Beijing), Beijing 102249, China*

https://doi.org/10.1021/acsomega.1c02952
ACS Omega 2021, 6, 23243−23261

Binbin Zhao − *State Key Laboratory of Petroleum Resources and Prospecting, China University of Petroleum (Beijing), Beijing 102249, China*

Complete contact information is available at: https://pubs.acs.org/10.1021/acsomega.1c02952

Author Contributions

J.W. wrote the main content, drew diagrams, and designed and operated the main experiments. S.Y. put forward research questions and main research ideas. B.G. conducted high-pressure mercury intrusion experiments and assisted in core classification and data interpretation. Y.C. was responsible for part of the translation work. W.Z., K.G., and Z.W. provided experimental materials and financial support. L.Q. assisted in the centrifugal experiment. W.D. participated in the literature research. Z.B. assisted in the nuclear magnetic resonance experiment. All authors reviewed the manuscript.

Notes

The authors declare no competing financial interest.

■ ACKNOWLEDGMENTS

This work was financially supported by the "973" Program "Basic Research on the Efficient Development of Terrestrial Tight Oil" Sub-project 4: "Research on the Mechanism and Method of Enhancing Tight Oil Reservoir Recovery" (2015CB250904) and the National Natural Science Foundation of China "Tight Oil Reservoir Matrix Imbibition Law And Crude Oil Production Mechanism Research" (51574257).

■ REFERENCES

(1) Mackenzie, F. T.; Veizer, J. *Evolution of Sedimentary Rocks*; Norton: New York. 2003, DOI: 10.1016/B0-08-043751-6/07103-6.

(2) Xiao, M.; Yuan, X.; Wu, S.; Cao, Z.; Tang, Y.; Xie, Z.; Wang, R. Conglomerate Reservoir Characteristics of and Main Controlling Factors for the Baikouquan Formation, Mahu sag, Junggar Basin. *Earth Sci. Front.* **2019**, *26*, 212−224.

(3) Zhi, D.; Tang, Y.; Zheng, M.; Guo, W.; Wu, T.; Zou, Z. Discovery, Distribution and Exploration Practice of Large Oil Provinces of Above-source Conglomerate in Mahu Sag. *Xinjiang Pet. Geol.* **2018**, *39*, 1−8.

(4) Li, G.; Qin, J.; Xian, C.; Fan, X.; Zhang, J.; Ding, Y. Theoretical understandings, key technologies and practices of tight conglomerate oilfield efficient development: A case study of the Mahu oilfield, Junggar Basin, NW China. *Pet. Explor. Dev.* **2020**, *47*, 1275−1290.

(5) Yang, Y. Analysis of Pore Type and Its Main Controlling Factors of Sand-Conglomerate Reservoirs in the Western Slope of Mahu, Junggar Basin. Yangtze univ., 2018.

(6) Miall, A. D. Architectural-Element Analysis: A New Method of Facies Analysis Applied to Fluvial Deposits. *Earth-Sci. Rev.* **1985**, *22*, 261−308.

(7) Miall, A. D. A Review of the Braided River Depositional Environment. *Earth-Sci. Rev.* **1977**, *13*, 1−62.

(8) Cant, D. J.; Ethier, V. G. Lithology-Dependent Diagenetic Control of Reservoir Properties of Conglomerates, Falher Member, Elmworth Field, Alberta. *Am. Assoc. Pet. Geol., Bull.* **1984**, *68*, 1044−1054.

(9) Hart, B. S.; Plint, A. G. Stratigraphy and Sedimentology of Shoreface and Fluvial Conglomerates: Insights from the Cardium Formation in NW Alberta and Adjacent British Columbia. *Bull. Can. Pet. Geol.* **2003**, *51*, 437−464.

(10) Ernando, Z.; Fathoni, A. *Volcanic Reservoir Characterization of Jatibarang Formation Based on an Integrated Study of Petrography, Core, FMI, and Well Log*; Indones. Pet. Assoc.: 2011.

(11) Zhang, K.; Wu, S.; Zhong, Y.; Shi, L. Modal Distribution of Pore-Throat Size in Sandy Conglomerates from an Alluvial Fan Environment: Lower Karamay Formation, Junggar Basin, West China. *Mar. Pet. Geol.* **2020**, *117*, 104391.

(12) Wang, Y. Z.; Mao, C. Diagenesis of the Cretaceous Glutenite and Its Control on the Reservoir Porosity in the Fangzheng Depression, Northeast China. *Environ. Earth Sci.* **2020**, *79*, 496.

(13) Zhang, C.; Song, X.; Wang, X.; Wang, X.; Zhao, K.; Shuang, Q.; Li, S. Origin and Depositional Characteristics of Supported Conglomerates. *Pet. Explor. Dev.* **2020**, *47*, 292.

(14) Chen, M.; Dai, J.; Liu, X.; Kuang, Y.; Qin, M.; Wang, Z. Contributions of Pore-throat Size Distribution to Reservoir Quality and Fluid Distribution from NMR and MIP in Tight Sandy Conglomerate Reservoirs. *Arabian J. Geosci.* **2019**, *12*, 9.

(15) Gao, H.; Wang, Y.; Xie, Y.; Ni, J.; Li, T.; Wang, C.; Xue, J. Imbibition and Oil Recovery Mechanism of Fracturing Fluids in Tight Sandstone Reservoirs. *ACS Omega* **2021**, *6*, 1991−2000.

(16) Li, P.; Jia, C.; Jin, Z.; Liu, Q.; Zheng, M.; Huang, Z. The Characteristics of Movable Fluid in the Triassic Lacustrine Tight Oil Reservoir: A Case Study of the Chang 7 Member of Xin'anbian Block, Ordos Basin, China. *Mar. Pet. Geol.* **2019**, *102*, 126−137.

(17) Lyu, C.; Ning, Z.; Wang, Q.; Chen, M. Application of NMR T_2 to Pore Size Distribution and Movable Fluid Distribution in Tight Sandstones. *Energy Fuels* **2018**, *32*, 1395−1405.

(18) Yao, Y.; Liu, D. Comparison of Low-Field NMR and Mercury Intrusion Porosimetry in Characterizing Pore Size Distributions of Coals. *Fuel* **2012**, *95*, 152−158.

(19) Zhang, Y.; Ge, H.; Shen, Y.; Jia, L.; Wang, J. Evaluating the potential for oil recovery by imbibition and time-delay effect in tight reservoirs during shut-in. *J. Pet. Sci. Eng.* **2020**, *184*, 106557.

(20) Purcell, W. R. Capillary Pressures - Their Measurement Using Mercury and the Calculation of Permeability Therefrom. *J Pet Technol* **1949**, *186*, 39−48.

(21) Thomeer, J. H. M. Introduction of a Pore Geometrical Factor Defined by the Capillary Pressure Curve. *J. Pet. Technol.* **1960**, *12*, 73−77.

(22) Abell, A. B.; Willis, K. L.; Lange, D. A. Mercury Intrusion Porosimetry and Image Analysis of Cement-Based Materials. *J. Colloid Interface Sci.* **1999**, *211*, 39−44.

(23) Zhang, W.; Ning, Z.; Wang, B. Experimental investigation of the variations in the pore structure of tight sandstones subjected to an electric field. *J. Pet. Sci. Eng.* **2021**, *204*, 108690.

(24) Zhao, Y.; Lin, B.; Liu, T.; Zheng, Y.; Sun, Y.; Zhang, G.; Li, Q. Multifractal Analysis of Coal Pore Structure Based on NMR Experiment: A New Method for Predicting T_2 cutoff Value. *Fuel* **2021**, *283*, 119338.

(25) Qing, J.; Yan, J.; Wang, J.; Hu, Q.; Wang, M.; Feng, S.; Geng, B.; Chao, J. Effects of mineralogy on pore structure and fluid flow capacity of deeply buried sandstone reservoirs with a case study in the Junggar Basin, East China. *J. Pet. Sci. Eng.* **2021**, *189*, 106986.

(26) Yang, F.; Xu, S.; Hao, F.; Hu, B.; Zhang, B.; Shu, Z.; Long, S. Petrophysical characteristics of shales with different lithofacies in Jiaoshiba area, Sichuan Basin, China: Implications for shale gas accumulation mechanism. *Mar. Pet. Geol.* **2019**, *109*, 394−407.

(27) Lin, T.; Wei, H. X.; Xie, Y. N. Using Throat Parametre to Assess Tight Sandstone Gas Reservoir: A Case Study of Dibei Tight Sandstone Gas in the East of Kuqa Depression. *Acta Sedimentol. Sin.* **2016**, *34*, 983−990.

(28) Wang, W.; Yue, D.; Eriksson, K. A.; Liu, X.; Liang, X.; Qu, X.; Xie, Q. Qualitative and Quantitative Characterization of Multiple Factors that Influence Movable Fluid Saturation in Lacustrine Deep-Water Gravity-Flow Tight Sandstones from the Yanchang Formation, Southern Ordos Basin, China. *Mar. Pet. Geol.* **2020**, *121*, 104625.

(29) Qiao, J.; Zeng, J.; Jiang, S.; Zhang, Y.; Feng, S.; Feng, X.; Hu, H. Insights into the Pore Structure and Implications for Fluid Flow Capacity of Tight Gas Sandstone: A Case Study in the Upper Paleozoic of the Ordos Basin. *Mar. Pet. Geol.* **2020**, *118*, 104439.

(30) Tian, W.; Lu, S.; Huang, W.; Wang, W.; Li, J.; Gao, Y.; Zhan, Z.; Sun, Y. Quantifying the Control of Pore Types on Fluid Mobility in Low-Permeability Conglomerates by Integrating Various Experiments. *Fuel* **2020**, *275*, 117835.

(31) Tian, W.; Lu, S.; Huang, W.; Wang, S.; Gao, Y.; Wang, W.; Li, J.; Xu, J.; Zhan, Z. Study on the Full-Range Pore Size Distribution and the

Movable Oil Distribution in Glutenite. *Energy Fuels* **2019**, *33*, 7028−7042.
(32) Li, W.; Wang, W.; Lu, S.; Xue, H. Quantitative Characterization on Shale-Hosted Oil Re-servoir : A Case Study of Argillaceous Dolomite Reservoir in the Jianghan Basin. *Fuel* **2017**, *206*, 690−700.
(33) Alfi, M.; Barrufet, M.; Killough, J. Effect of Pore Sizes on Composition Distribution and Enhance Recovery from Liquid Shale—Molecular Sieving in Low Permeability Reservoirs. *Fuel* **2019**, *235*, 1555−1564.
(34) Phinn, S.; Stanford, M.; Scarth, P.; Murray, A. T.; Shyy, P. T. Monitoring the Composition and Form of Urban Environments Based on the Vegetation Impervious Surface-Soil (VIS) Model by Sub-Pixel Analysis Techniques. *Int. J. Remote Sens.* **2002**, *23*, 4131−4153.
(35) Weng, Q.; Lu, D. A Sub-Pixel Analysis of Urbanization Effect on Land Surface Temperature and Its Interplay with Impervious Surface and Vegetation Coverage in Indianapolis, United States. *Int. J. Appl. Earth Obs. Geoinf.* **2008**, *10*, 68−83.
(36) Jiang, W.; Imin, A.; Wang, X.; Wang, T.; Guo, W. Geochemical Characterization and Quantitative Identification of Mixed-Source Oils From the Baikouquan and Lower Wuerhe Formations in the Eastern Slope of the Mahu Sag, Junggar Basin, NW China. *J. Pet. Sci. Eng.* **2020**, *191*, 107175.
(37) Nouidar, M.; Chellaï, E. H. Facies and Sequence Stratigraphy of a Late Barremian Wave-Dominated Deltaic Deposit, Agadir Basin, Morocco. *Sediment. Geol.* **2002**, *150*, 375−384.
(38) Tang, Y.; Guo, W.; Wang, X.; Bao, H.; Wu, H. A New Breakthrough in Exploration of Large Conglomerate Oil Province in Mahu Sag and Its Implications. *Xingjiang Pet. Geol.* **2019**, *40*, 127−137.
(39) Chen, N.; Guo, M.; Meng, X. Pore Structures and Controlling Factors of Middle Permian-Lower Triassic Sandy Conglomerates in Northwestern Margin of Junggar Basin. *Xinjiang. Pet. Geol.* **2016**, *4*, 401−408.
(40) Qiu, Z.; He, N.; Wang, H.; Li, X.; Li, T.; Zhou, Q.; Shi, L. The Sedimentological Reservoir Characteristics of the Jurassic Sangonghe Formation, Southern Mahu Slope, Junggar Basin, Northwestern China. *Geol. J.* **2021**, *56*, 1478−1495.
(41) Song, F.; Su, N.; Kong, X.; Liu, C.; Song, C. Sedimentary Characteristics of Humid Alluvial Fan and Its Control on Hydrocarbon Accumulation: A Case Study on the Northern Margin of the Junggar Basin, West China. *J. Pet. Sci. Eng.* **2020**, 187.
(42) Qu, J.; Zhang, L.; Wu, J.; You, X. Characteristics of Sandy Conglomerate Reservoirs and Controlling Factors on Physical Properties of Baikouquan Formation in the Western Slope of Mahu Sag, Junggar Basin. *Xinjiang. Pet. Geol.* **2017**, *38*, 1−6.
(43) Li, A.; Ren, X.; Wang, G.; Wang, Y.; Jiang, K. Characterization of Pore Structure of Low Permeability Reservoirs Using a Nuclear Magnetic Resonance Method. *J. China Univ. Pet. Ed. Nat. Sci.* **2015**, *39*, 92−98.
(44) Li, W.; Gao, Z.; Peng, D. Lateral Accretion Cross—Bedding: The Main Type of Sedimentary Structures in the Braided Channel. *Exp. Pet. Geol.* **1996**, *18*, 298−302.
(45) Krumbein, W. C. Size Frequency Distributions of Sediments and the Normal Phi Curve. *J. Sediment. Res.* **1938**, *8*, 84−90.
(46) Clarkson, C. R.; Solano, N.; Bustin, R. M.; Bustin, A. M. M.; Chalmers, G. R. L.; He, L.; Melnichenko, Y. B.; Radliński, A. P.; Blach, T. P. Pore Structure Characterization of North American Shale Gas Reservoirs Using USANS/SANS, Gas Adsorption, and Mercury Intrusion. *Fuel* **2013**, *103*, 606−616.
(47) Lu, Y.; Liu, K. Pore Structure Characterization of Eocene Low-Permeability Sandstones via Fractal Analysis and Machine Learning: An Example from the Dongying Depression, Bohai Bay Basin, China. *ACS omega* **2021**, *6*, 11693−11710.
(48) Rieke, H. H.; Chilingarian, G. V. Compaction of Argillaceous Sediments. *Developments in Petroleum Science*; Elsevier: 1974.
(49) Wang, M.; Xie, J.; Guo, F.; Zhou, Y.; Yang, X.; Meng, Z. Determination of NMR T_2 Cutoff and CT Scanning for Pore Structure Evaluation in Mixed Siliciclastic-Carbonate Rocks before and after Acidification. *Energies* **2020**, *13*, 1338.
(50) Zheng, S.; Yao, Y.; Elsworth, D.; Wang, B.; Liu, Y. A Novel Pore Size Classification Method of Coals: Investigation Based on NMR Relaxation. *J. Nat. Gas Sci. Eng.* **2020**, *81*, 103466.
(51) Shi, G.; Kou, G.; Du, S.; Wei, Y.; Li, T. What Role Would the Pores Related to Brittle Minerals Play in the Process of Oil Migration and Oil & Water Two-Phase Imbibition? *Energy Rep.* **2020**, *6*, 1213−1223.
(52) Zhou, T.; Wu, C.; Shi, Z.; Wang, J.; Zhu, W.; Yuan, B.; Yang, D. Multi-Scale Quantitative Characterization of Pore Distribution Networks in Tight Sandstone by integrating FE-SEM, HPMI, and NMR with the Constrained Least Squares Algorithm. *Energies* **2019**, *12*, 3514.
(53) Lu, D.; Weng, Q. Use of Impervious Surface in Urban Land-Use Classification. *Remote Sens. Environ.* **2006**, *102*, 146−160.

https://doi.org/10.1021/acsomega.1c02952
ACS Omega 2021, 6, 23243−23261